Dimensional Model Reduction in Non-linear Finite Element Dynamics of Solids and Structures

P. Krysl[1,*], S. Lall[2], J. E. Marsden[2]

California Institute of Technology,
[1] *Computer Science, Mail code 256-80*
[2] *Control and Dynamical Systems, Mail code 107-81*
Pasadena, CA 91125.
pkrysl@cs.caltech.edu, sanj@cds.caltech.edu, marsden@cds.caltech.edu

KEY WORDS: Solid dynamics, finite element method, Ritz basis, model dimension reduction, empirical eigenvectors, Karhunen-Loève expansion

SUMMARY

A general approach to the dimensional reduction of non-linear finite element models of solid dynamics is presented. For the Newmark implicit time-discretization, the computationally most expensive phase is the repeated solution of the system of linear equations for displacement increments. To deal with this, it is shown how the problem can be formulated in an approximation (Ritz) basis of much smaller dimension. Similarly, the explicit Newmark algorithm can be also written in a reduced-dimension basis, and the computation time savings in that case follow from an increase in the stable time step length.

In addition, the empirical eigenvectors are proposed as the basis in which to expand the incremental problem. This basis achieves approximation optimality by using computational data for the response of the full model in time to construct a reduced basis which reproduces the full system in a statistical sense. Because of this "global" time viewpoint, the basis need not be updated as with reduced bases computed from a linearization of the full finite element model.

If the dynamics of a finite element model is expressed in terms of a small number of basis vectors, the asymptotic cost of the solution with the reduced model is lowered and optimal scalability of the computational algorithm with the size of the model is achieved. At the same time, numerical experiments indicate that by using reduced models, substantial savings can be achieved even in the pre-asymptotic range. Furthermore, the algorithm parallelizes very efficiently.

The method we present is expected to become a useful tool in applications requiring a large number of repeated non-linear solid dynamics simulations, such as convergence studies, design optimization, and design of controllers of mechanical systems.

INTRODUCTION

In general, finite element (FE) analysis of dynamic non-linear deformations of solids and structures can be rather expensive, especially in situations when one requires many repeated trials, as often happens in design and control applications. Explicit time discretization avoids storage of large matrices and repeated costly solution of systems of linear equations, but is limited by its conditional stability.

Implicit time stepping algorithms require repeated solutions of large systems of linear equations, which consume considerable resources both in terms of the computation time and in terms of the data storage requirements.

The standard FE approximation basis is non-optimal in the sense that the coherence and relatively simple large scale structures of the displacement fields that one often sees are not exploited. For instance, consider linear forced vibrations of solids: Decomposition of the displacement field into vibration modes is optimal in the sense that, depending on the frequency content of the loading, a relatively small number of modes is sufficient to describe the motion for a given error tolerance.

The principal idea of dimensional model reduction is to find a small number of generalized coordinates in which to express the dynamics, ideally with some bounds on the truncation error. One way of applying this idea in the context of FE models is a transition from the collection of individual nodal basis functions to several linear combinations of the nodal basis functions (modes, or generalized coordinates). The question is how to compute the amplitudes of the FE basis functions for the needed modes, and how to integrate the reduced dynamical system in time. Recent results on model reduction of general Lagrangian systems were developed in [23], while the present paper focusses on using those methods for reduction of finite-element models.

Before proceeding with a short exposition of prior research, a terminological note is in order. A globally supported generalized coordinate function is commonly called a ***Ritz function***. This notation appears to have been chosen to contrast this type of functions with the standard compact-support FE basis functions.

In what follows, attention is given primarily to reduction of the incremental form of the equations of motion. (The only model reduction alternative so far, the pseudo-force method as proposed by Stricklin et al [42], is limited to moderate non-linearities.)

Related Literature. A recent overview of tangent spectrum methods in non-linear mechanics was given by Leger and Dussault [24]. Nickell's paper [30] is often cited in connection with extending the principle of mode superposition of linear vibration analysis to linearizations of non-linear dynamic motion (local mode superposition). The incremental motion problem is solved in the modal basis derived from the tangent eigenvibration problem. As expected, the basis needs to be changed quite frequently, because the linearization also changes. Repeated solutions of the eigenvibration problem are costly. Even more importantly, it should be noted that a change of approximation basis in general means that a time-dependent constraint had been introduced, which may change dramatically the behaviour of the model. Subsequent work was aimed at improvements in the first of these two areas; the second problem had not been realized.

Almroth, Stern and Brogan suggested use of the corrective displacement in the first equilibrium iteration as the Ritz vector to enhance the current basis [1]. Noor and Peters used the path derivatives of the current displacement solution as generalized coordinates [32], and Noor also proposed using a mix of linear vibration eigenmodes combined with "steady-state" modes (eigenmodes obtained for structures with static pre-stress) [31].

Wilson, Yuan and Dickens suggested an algorithm generating mass-orthogonal (Krylov) vectors by starting from the static displacement [44]. A distinct advantage of this algorithm is that no eigenvalue problem needs to be solved. Also, it accounts directly for the spatial distribution of the load.

Idelsohn and Cardona proposed using current tangent eigenvibration modes with their approximate time derivatives [16]. Each change of the reduced basis was found to lead to an accumulation of error, because of the necessity to project the current displacements onto the new basis as the initial conditions for the time integration. Idelsohn and Cardona advanced the idea of using the load-dependent sequence of Ritz vectors with their derivatives with respect to the modal coefficients [15].

Chan and Hsiao proposed using the orthogonalized previous and current displacement vectors with some selected equilibrium iteration displacement vectors as the basis for non-linear static analyses [4]. The basis could be generated with little cost, and the results were of good quality. The main disadvantage is that the full model is needed for each re-generation of the reduced basis. Chang and Engblom used load-dependent Ritz vectors with some rudimentary ranking of the participation of the individual Ritz vectors in the response at any given time [5].

The error introduced as a result of using a small number of modes (***truncation error***) needs to be understood to make the technique practically useful. Some understanding is available for linear vibration problems: Kline explored truncation errors for linear systems approximated with reduced

Copyright © 2000 John Wiley & Sons, Ltd.

Prepared using nmeauth.cls

bases consisting of exact vibration modes and load-dependent Ritz vectors [21], and found that the residual error was composed of two sources, the first due to the inability of the truncated basis to reproduce the loading, and the second following from the failure of the reduced basis to reproduce the exact eigenvibration response of the full model. Joo, Wilson and Leger suggested truncation criteria for the load-dependent Ritz basis [18], and again the omission of the load components orthogonal to the modes included in the basis was related to the truncation error. This issue was further investigated by Ricles and Leger [34]. Ibrahimbegovic and Wilson presented a way of incorporating the frequency contents truncation criteria in the process of generating the Ritz vectors that span the Krylov subspace [14], and Xia and Humar enhanced the approximation properties of the load-dependent Ritz vectors by using a shift in the Krylov sequence generation derived from the predominant excitation frequency [46]. Cabos provided a posteriori error estimates for linear vibration problems discretized with Ritz load-dependent vectors generated by a block-Lanczos algorithm [3], and Balmès extended the concept of model dimension reduction to parametric families of reduced basis vectors [2]. Joo and Wilson described an application of the Ritz vectors in FE mesh adaptation for dynamic problems [17]. Compared to this wealth of results for linear systems, the understanding of the truncation error in non-linear dynamic analyses is limited.

For control problems involving general sets of ordinary differential equations, some related error-measures have been developed, particularly using the method of *balanced truncation*. In the linear case, these error-bounds were derived by Glover [9] and Enns [7]; for nonlinear systems, error-bounds have been developed by Wood [45] and Scherpen [35].

Organization of the Paper. Following a brief introduction to finite element modeling of deformations of nonlinear continua (or structures) in Section 1, the model dimension reduction approach is explained first for the implicit Newmark integrator (Section 2), and then for the explicit variant (Section 3). The empirical eigenvector basis is introduced in Section 4, which is followed by a short Section 5 on error estimation and adaptivity issues. Comparison with existing approaches is made in Section 6, and several illustrative examples of advantages and interesting features of the present technique are given in Section 7.

1. FORMULATION OF FE MODELS

Our setting is that of displacement-based finite element (FE) models of transient nonlinear deformation of general solids. The reference configuration of a three-dimensional body $\mathcal{B}^0 \subset \mathbb{R}^3$ is described in Cartesian coordinates by labeling material points with their position $\boldsymbol{X} \in \mathcal{B}^0$. The motion $\boldsymbol{\varphi} : \mathcal{B}^0 \to \mathcal{B}$ takes each reference point $\boldsymbol{X}$ to the current point $\boldsymbol{x} \in \mathcal{B}$; we write

$$\boldsymbol{x}(\boldsymbol{X}, t) = \boldsymbol{\varphi}(\boldsymbol{X}, t) = \boldsymbol{X} + \boldsymbol{u}(\boldsymbol{X}, t) \ , \tag{1}$$

where $\boldsymbol{u} \in \mathcal{C}$ is the displacement, which is to satisfy the essential boundary conditions on part of the boundary $\partial^u \mathcal{B}^0$:

$$\mathcal{C} = \left\{ \boldsymbol{u}(\boldsymbol{X}, t) : \ \mathcal{B}^0 \to \mathbb{R}^3 \ | \ \boldsymbol{u}(\boldsymbol{X}, t) = \bar{\boldsymbol{u}}(\boldsymbol{X}, t) \ \text{ on } \ \partial^u \mathcal{B}^0 \right\} \ , \tag{2}$$

where $\bar{\boldsymbol{u}}$ is given. Note that the boundary condition (2) is easily modified if only some components of the displacement vector are prescribed.

The equations of motion are obtained from the following standard weak form of the variational principle [28], stated on the reference configuration $\mathcal{B}^0$ in terms of the the displacement $\boldsymbol{u}$ and the 1st Piola-Kirchhoff stress tensor $\boldsymbol{P}$ as

$$\int_{\mathcal{B}^0} \rho^0 \ddot{\boldsymbol{u}} \cdot \boldsymbol{\eta} \, \mathrm{d}V = \int_{\mathcal{B}^0} \rho^0 \overline{\boldsymbol{b}} \cdot \boldsymbol{\eta} \, \mathrm{d}V - \int_{\mathcal{B}^0} \boldsymbol{P} \cdot \left(\boldsymbol{\nabla}^0 \otimes \boldsymbol{\eta} \right)^T \, \mathrm{d}V + \int_{\partial^t \mathcal{B}^0} \overline{\boldsymbol{t}} \cdot \boldsymbol{\eta} \, \mathrm{d}A \ , \tag{3}$$

where dot denotes material time derivative, ρ^0 is the mass density in the reference configuration, $\overline{\boldsymbol{b}}$ is the prescribed body load, $\boldsymbol{\eta}$ is the variation of the displacement, $\overline{\boldsymbol{t}}$ is the prescribed traction, and the vector gradient operator $\boldsymbol{\nabla}^0 \otimes$ is defined as

$$\left(\boldsymbol{\nabla}^0 \otimes \boldsymbol{v} \right)^T = \partial v_i / \partial X_j \boldsymbol{e}_i \otimes \boldsymbol{e}_j \ ,$$

Copyright © 2000 John Wiley & Sons, Ltd.

Prepared using nmeauth.cls

with $\boldsymbol{e}_k$ the Cartesian basis vectors, and X_j the components of the material point position vector $\boldsymbol{X}$.

The displacement variation $\boldsymbol{\eta} \in \mathcal{V}$ needs to satisfy the homogeneous essential boundary conditions

$$\mathcal{V} = \left\{ \boldsymbol{\eta}(\boldsymbol{X},t) \mid \boldsymbol{\eta}(\boldsymbol{X},t) = \boldsymbol{0} \ \text{ on } \ \partial^u \mathcal{B}^0 \right\} \ . \tag{4}$$

The deformation evolution is sought under given initial conditions on $\boldsymbol{u}$ and $\boldsymbol{P}$ which we write as follows:

$$\dot{\boldsymbol{u}}(\boldsymbol{X},0) = \bar{\boldsymbol{v}}(\boldsymbol{X}) \ , \qquad \boldsymbol{X} \in \mathcal{B}^0 \ , \tag{5}$$

and

$$\boldsymbol{P}(\boldsymbol{X},0) = \bar{\boldsymbol{P}}(\boldsymbol{X}) = \boldsymbol{\sigma}(\boldsymbol{X},0) \ , \qquad \boldsymbol{X} \in \mathcal{B}^0 \ . \tag{6}$$

Equation (3) may be re-written as

$$K(\boldsymbol{u},\boldsymbol{\eta}) = G^{\text{ext}}(\boldsymbol{u},\boldsymbol{\eta}) - G^{\text{int}}(\boldsymbol{u},\boldsymbol{\eta}) \ , \tag{7}$$

where

$$K(\boldsymbol{u},\boldsymbol{\eta}) \quad = \int_{\mathcal{B}^0} \rho^0 \ddot{\boldsymbol{u}} \cdot \boldsymbol{\eta} \, \mathrm{d}V \ , \tag{8a}$$

$$G^{\text{ext}}(\boldsymbol{u},\boldsymbol{\eta}) = \int_{\mathcal{B}^0} \rho^0 \overline{\boldsymbol{b}} \cdot \boldsymbol{\eta} \, \mathrm{d}V + \int_{\partial^t \mathcal{B}^0} \overline{\boldsymbol{t}} \cdot \boldsymbol{\eta} \, \mathrm{d}A \ , \tag{8b}$$

$$G^{\text{int}}(\boldsymbol{u},\boldsymbol{\eta}) = \int_{\mathcal{B}^0} \boldsymbol{P} \cdot \left(\boldsymbol{\nabla}^0 \otimes \boldsymbol{\eta} \right)^T \, \mathrm{d}V \ . \tag{8c}$$

Finite Element Galerkin Approximation. The displacement $\boldsymbol{u}$ and the displacement variation $\boldsymbol{\eta}$ are approximated in the FE basis as

$$\boldsymbol{u}_h(\boldsymbol{X},t) = \sum_I^N N_I(\boldsymbol{X}) \boldsymbol{u}_I(t) \quad \text{and} \quad \boldsymbol{\eta}_h(\boldsymbol{X},t) = \sum_I^N N_I(\boldsymbol{X}) \boldsymbol{\eta}_I(t) \ , \tag{9}$$

where $N_I(\boldsymbol{X})$ is the FE basis function, and $\boldsymbol{u}_I(t)$ and $\boldsymbol{\eta}_I(t)$ represent the nodal parameters. The configuration space $\mathcal{C}$ is approximated as

$$\mathcal{C}_h = \left\{ \boldsymbol{u}_h(\boldsymbol{X},t) \ \middle| \ \boldsymbol{u}_h(\boldsymbol{X},t) = \sum_I N_I(\boldsymbol{X}) \bar{\boldsymbol{u}}(\boldsymbol{X}_I,t) \text{ on } \partial^u \mathcal{B}_h^0 \right\} \ , \tag{10}$$

where $\partial^u \mathcal{B}_h^0$ is the FE discretization of the boundary $\partial^u \mathcal{B}^0$, and similarly the space of variations $\mathcal{V}$:

$$\mathcal{V}_h = \left\{ \boldsymbol{\eta}_h(\boldsymbol{X},t) \mid \boldsymbol{\eta}_h(\boldsymbol{X},t) = \boldsymbol{0} \ \text{ on } \ \partial^u \mathcal{B}_h^0 \right\} \ . \tag{11}$$

Substitution of (9) into (7) yields the discrete form of the variational principle

$$K_h(\boldsymbol{u},\boldsymbol{\eta}) = G_h^{\text{ext}}(\boldsymbol{u},\boldsymbol{\eta}) - G_h^{\text{int}}(\boldsymbol{u},\boldsymbol{\eta}) \ , \tag{12}$$

where

$$\begin{aligned} K_h(\boldsymbol{u},\boldsymbol{\eta}) \quad &= \quad \sum_{I,J}^N \boldsymbol{\eta}_I \cdot \boldsymbol{M}_{IJ} \cdot \ddot{\boldsymbol{u}}_J \ , \\ G_h^{\text{ext}}(\boldsymbol{u},\boldsymbol{\eta}) \quad &= \quad \sum_I^N \boldsymbol{\eta}_I \cdot \boldsymbol{f}_I^{\text{ext}}(\boldsymbol{u}) \ , \\ G_h^{\text{int}}(\boldsymbol{u},\boldsymbol{\eta}) \quad &= \quad \sum_I^N \boldsymbol{\eta}_I \cdot \boldsymbol{f}_I^{\text{int}}(\boldsymbol{u}) \ . \end{aligned}$$

Equation (12) is equivalent to the dynamic equilibrium equation

$$\sum_J^N \boldsymbol{M}_{IJ} \cdot \ddot{\boldsymbol{u}}_J = \boldsymbol{f}_I^{\text{ext}} - \boldsymbol{f}_I^{\text{int}} \tag{13}$$

for all I, where $\boldsymbol{M}_{IJ}$ is the mass matrix linking nodes I and J, and $\boldsymbol{f}_I^{\text{ext}}$ and $\boldsymbol{f}_I^{\text{int}}$ are the vectors of impressed (external) and restoring (internal) forces acting on node I.

Copyright © 2000 John Wiley & Sons, Ltd.

Prepared using nmeauth.cls

2. MODEL DIMENSION REDUCTION FOR IMPLICIT NEWMARK INTEGRATION

Equations (13) are a system of nonlinear second-order ordinary differential equations, which is commonly integrated in time either by an explicit integrator (central differences), or by one of the popular implicit integrators. The Newmark time-stepping algorithm is widely used in structural dynamics, and has been recently shown to be a variational integrator [19]. Equation (13) discretized in time with this algorithm reads

$$\begin{aligned} \boldsymbol{M}\boldsymbol{a}_{t+\Delta t} &= \boldsymbol{f}^{\text{ext}}_{t+\Delta t} - \boldsymbol{f}^{\text{int}}_{t+\Delta t} \\ \boldsymbol{u}_{t+\Delta t} &= \boldsymbol{u}_t + \Delta t \boldsymbol{v}_t + \frac{\Delta t^2}{2}\left[(1-2\beta)\boldsymbol{a}_t + 2\beta \boldsymbol{a}_{t+\Delta t}\right] \\ \boldsymbol{v}_{t+\Delta t} &= \boldsymbol{v}_t + \Delta t\left[(1-\gamma)\boldsymbol{a}_t + \gamma \boldsymbol{a}_{t+\Delta t}\right] \end{aligned} \tag{14}$$

where $\boldsymbol{u}_\tau$, $\boldsymbol{v}_\tau$ and $\boldsymbol{a}_\tau$ are discrete-time analogs of $\boldsymbol{u}(\tau)$, $\dot{\boldsymbol{u}}(\tau)$, and $\ddot{\boldsymbol{u}}(\tau)$; $\boldsymbol{M}$ is the time-independent global mass matrix. We set $\gamma = 1/2$ for second order accuracy, and $\beta \geq 1/4$.

The time stepping algorithm (14) is customarily implemented with a Newton-Raphson equilibrium iteration loop. By linearizing G_h^{int} from (8a) we obtain the tangent stiffness matrix

$$L\left[G_h^{\text{int}}(\boldsymbol{u},\boldsymbol{\eta}),\Delta\boldsymbol{u}\right] = \sum_I^N \sum_J^N \boldsymbol{\eta}_I \cdot \boldsymbol{K}_{IJ} \cdot \Delta\boldsymbol{u}_J \tag{15}$$

where $L\left[\xi,\boldsymbol{v}\right]$ is the linearization of ξ in the direction of $\boldsymbol{v}$. Here, $\boldsymbol{K}_{IJ}$ is the submatrix of the tangent stiffness linking nodes I and J, which may be expressed as sum of of two matrices, $\boldsymbol{K}^{\text{m}}_{IJ}$ and $\boldsymbol{K}^{\sigma}_{IJ}$. The first part corresponds to the constitutive tangent stiffness

$$\sum_I^N \sum_J^N \boldsymbol{\eta}_I \cdot \boldsymbol{K}^{\text{m}}_{IJ} \cdot \Delta\boldsymbol{u}_J = \int_{\mathcal{B}^0} L\left[\boldsymbol{E}(\boldsymbol{u}),\boldsymbol{\eta}\right] \cdot \mathcal{C} \cdot \; L\left[\boldsymbol{E}(\boldsymbol{u}),\Delta\boldsymbol{u}\right] \,\mathrm{d}V \tag{16}$$

where $\mathcal{C}$ is the constitutive tangent tensor, and $\boldsymbol{E}$ is the Green-Lagrange strain tensor,

$$\boldsymbol{E}(\boldsymbol{u}) = \frac{1}{2}\left[\left(\boldsymbol{\nabla}^0 \otimes \boldsymbol{u}\right)^T + \boldsymbol{\nabla}^0 \otimes \boldsymbol{u} + \left(\boldsymbol{\nabla}^0 \otimes \boldsymbol{u}\right)^T \cdot \boldsymbol{\nabla}^0 \otimes \boldsymbol{u}\right] \; .$$

The constitutive tangent stiffness should in fact be formulated by linearization of a particular stress update algorithm, see for instance Reference [37], but the above simplification saves space while not affecting our conclusions regarding model reduction.

The second constituent incorporates the effect of stress in the current state

$$\sum_I^N \sum_J^N \boldsymbol{\eta}_I \cdot \boldsymbol{K}^{\sigma}_{IJ} \cdot \Delta\boldsymbol{u}_J = \int_{\mathcal{B}^0} \left(\boldsymbol{\nabla}^0 \otimes \boldsymbol{u}\right)^T \boldsymbol{P} : \left(\boldsymbol{\nabla}^0 \otimes \boldsymbol{\eta}\right) \cdot \left(\boldsymbol{\nabla}^0 \otimes \Delta\boldsymbol{u}\right)^T \,\mathrm{d}V \; . \tag{17}$$

Linearization of the $K_h(\boldsymbol{u},\boldsymbol{\eta})$ term is easily established as

$$L\left[K_h(\boldsymbol{u},\boldsymbol{\eta}),\Delta\boldsymbol{u}\right] = \sum_{I,J}^N \boldsymbol{\eta}_I \cdot \boldsymbol{M}_{IJ} \cdot \Delta\ddot{\boldsymbol{u}}_J \; . \tag{18}$$

If we assume that the loads are configuration independent, that is if

$$L\left[G_h^{\text{ext}}(\boldsymbol{u},\boldsymbol{\eta}),\Delta\boldsymbol{u}\right] = 0 \; ,$$

the linearization of (12) is expressed as

$$\sum_{I,J}^N \boldsymbol{\eta}_I \cdot \boldsymbol{M}_{IJ} \cdot \Delta\ddot{\boldsymbol{u}}_J = \sum_{I,J}^N \boldsymbol{\eta}_I \cdot \boldsymbol{K}_{IJ} \cdot \Delta\boldsymbol{u}_J \; . \tag{19}$$

Copyright © 2000 John Wiley & Sons, Ltd.

Prepared using nmeauth.cls

With these results, the Newmark algorithmic equations (14) including the Newton-Raphson equilibrium iteration loop can be cast in the well-known predictor-corrector form

$$
\begin{array}{lll}
i \leftarrow 0 & & \\
\left.\begin{array}{rcl}
\boldsymbol{u}_{t+\Delta t}^{(i)} & = & \boldsymbol{u}_t, \\
\boldsymbol{a}_{t+\Delta t}^{(i)} & = & -\dfrac{1}{\beta \Delta t}\boldsymbol{v}_t + \left(1 - \dfrac{1}{2\beta}\right)\boldsymbol{a}_t, \\
\boldsymbol{v}_{t+\Delta t}^{(i)} & = & \boldsymbol{v}_t + \Delta t\left[(1-\gamma)\,\boldsymbol{a}_t + \gamma \boldsymbol{a}_{t+\Delta t}^{(i)}\right]
\end{array}\right\} & \text{predictor} \\
i \leftarrow i+1 & & \text{next iteration} \\
\boldsymbol{K}^{\mathrm{eff}(i)} = \dfrac{1}{\beta \Delta t^2}\boldsymbol{M} + \boldsymbol{K}^{\mathrm{m}(i)} + \boldsymbol{K}^{\sigma(i)} & & \text{effective stiffness} \\
\boldsymbol{R}^{(i)} = \boldsymbol{M}\boldsymbol{a}_{t+\Delta t}^{(i)} - \boldsymbol{f}_{t+\Delta t}^{\mathrm{ext}(i)} + \boldsymbol{f}_{t+\Delta t}^{\mathrm{int}(i)} & & \text{residual} \\
\Delta \boldsymbol{u}^{(i)} = \boldsymbol{K}^{\mathrm{eff}(i)^{-1}}\boldsymbol{R}^{(i)} & & \text{displ. increment} \\
\left.\begin{array}{rcl}
\boldsymbol{u}_{t+\Delta t}^{(i)} & = & \boldsymbol{u}_{t+\Delta t}^{(i-1)} + \Delta \boldsymbol{u}^{(i)} \\
\boldsymbol{v}_{t+\Delta t}^{(i)} & = & \boldsymbol{v}_{t+\Delta t}^{(i-1)} + \dfrac{\gamma}{\beta \Delta t}\Delta \boldsymbol{u}^{(i)} \\
\boldsymbol{a}_{t+\Delta t}^{(i)} & = & \boldsymbol{a}_{t+\Delta t}^{(i-1)} + \dfrac{1}{\beta \Delta t^2}\Delta \boldsymbol{u}^{(i)}
\end{array}\right\} & \text{corrector} \\
\text{If } \; ||\boldsymbol{R}^{(i)}|| > \epsilon ||\boldsymbol{R}^{(0)}|| \text{ repeat for next iteration;} & & \\
\text{else } \; t \leftarrow t + \Delta t \text{ and go to the top.} & &
\end{array}
\tag{20}
$$

The iteration is broken off if the norm of the force residual in iteration i drops below a certain fraction, $0 < \epsilon \ll 1$, of the residual computed from the predictor (iteration 0).

Cost Analysis. The computational cost of the algorithm (20) may be expressed in terms of the total number of FE nodes, N (assuming the number of finite elements, and the number of degrees of freedom per node are constant multiples of N). Table I summarizes the per operation costs. The two most expensive operations, in terms of both computation time and storage, are the tangent stiffness assembly and the solution for the displacement increment. Even though the effective stiffness matrix $\boldsymbol{K}^{\mathrm{eff}(i)}$ is sparse, it may be unsymmetric, possibly badly conditioned. Therefore, its storage and the solution of the system of linear equations is often very expensive compared to the other operations. Perhaps most importantly, scalability of the overall algorithm with the growing size of the discrete system is adversely affected: The solution cost of the sparse system of linear equations grows as $O\left[s(N)\right] \geq O(N)$, where $s(N)$ is a function depending on the solver characteristics. For instance, for a direct solution of a banded system $s(N) = N^2$; for iterative solvers, each iteration costs $O(N)$, and the number of iterations in general depends on N, hence again $s(N) \geq N$.

Operation	Cost
Predictor	$O(N)$
Force assembly	$O(N)$
Tangent assembly	$O(N)$
Solve for displ. incr.	$O[s(N)]$
Configuration update	$O(N)$

Table I. Asymptotic cost of the Newmark implicit algorithm operations

Copyright © 2000 John Wiley & Sons, Ltd.

Prepared using nmeauth.cls

Reduced Dimensional Basis. The main idea of model dimension reduction as applied to the system of equations (14) is to find a spatial representation of the primary variable $\boldsymbol{u}$, which would ensure the response of the full and reduced models to be close in a certain sense, and which would be at the same time much terser than the full FE model. In other words, we would like to find a representation minimizing the number of degrees of freedom which need to be included in the computation to reach a certain error level (measured with respect to the full FE model).

The full FE model represents the configuration in the FE space $\mathcal{C}_h$. It seems quite natural to look for a more succinct representation of the configuration $\widehat{\mathcal{C}}_h$ in a linear subspace of the full FE space

$$\widehat{\mathcal{C}}_h \subset \mathcal{C}_h \ . \tag{21}$$

The reduced configuration space $\widehat{\mathcal{C}}_h$ is represented as follows:

$$\widehat{\mathcal{C}}_h = \left\{ \widehat{\boldsymbol{u}}_h(\boldsymbol{X},t) \mid \widehat{\boldsymbol{u}}_h(\boldsymbol{X},t) = \boldsymbol{u}_h(\boldsymbol{X},t) \ \text{ on } \ \partial^u \mathcal{B}_h^0 \right\} \ , \tag{22}$$

with

$$\widehat{\boldsymbol{u}}_h(\boldsymbol{X},t) = \sum_j^M \boldsymbol{\phi}^j(\boldsymbol{X}) p_j(t) \ , \tag{23}$$

where $p_j(t)$ are the mode coefficients, and $M \ll N$ is the number of modes. The (Ritz) basis functions $\boldsymbol{\phi}^j(\boldsymbol{X})$ are, by virtue of (21), expressible as linear combinations of the functions $N_I(\boldsymbol{X})$

$$\boldsymbol{\phi}^j(\boldsymbol{X}) = \sum_I^N N_I(\boldsymbol{X}) \boldsymbol{\phi}_I^j \ , \tag{24}$$

where the coefficient vectors $\boldsymbol{\phi}_I^j$ are given a priori. Their choice is crucial to the success of the reduction process, and we discuss one approach to their computation in Section 4.

The reduced configuration space $\widehat{\mathcal{C}}_h$ conforms to the boundary condition (22) if

$$\widehat{\boldsymbol{u}}_h(\boldsymbol{X},t) \Big|_{\partial^u \mathcal{B}_h^0} = \boldsymbol{u}_h(\boldsymbol{X},t) \Big|_{\partial^u \mathcal{B}_h^0} \ , \tag{25}$$

i.e.

$$\sum_j^M \boldsymbol{\phi}^j(\boldsymbol{X}) p_j(t) = \sum_I N_I(\boldsymbol{X}) \bar{\boldsymbol{u}}(\boldsymbol{X}_I,t) \ \text{ on } \ \partial^u \mathcal{B}_h^0 \ . \tag{26}$$

Substituting (24), we get the condition

$$\sum_j^M \sum_I^N N_I(\boldsymbol{X}) \boldsymbol{\phi}_I^j p_j(t) = \sum_I N_I(\boldsymbol{X}) \bar{\boldsymbol{u}}(\boldsymbol{X}_I,t) \ \text{ on } \ \partial^u \mathcal{B}_h^0 \ , \tag{27}$$

which may be met provided

$$\sum_j^M \boldsymbol{\phi}_I^j p_j(t) = \bar{\boldsymbol{u}}(\boldsymbol{X}_I,t) \qquad \forall I \ , \tag{28}$$

for all time t. It is evident that Equation (28) will not be satisfied exactly for general inhomogeneous boundary conditions, since the mode mixing coefficients $p_j(t)$ are determined not only by the boundary conditions, but also (mainly) by the overall dynamics. On the other hand, Equation (28) is easily satisfied for the homogeneous constraints $\boldsymbol{u}(\boldsymbol{X},t) = \boldsymbol{0}$ by setting the coefficient vectors $\boldsymbol{\phi}_I^j$ identically equal to zero, $\boldsymbol{\phi}_I^j = \boldsymbol{0}$, for all the FE nodes I on the boundary $\partial^u \mathcal{B}_h^0$.

Copyright © 2000 John Wiley & Sons, Ltd.

Prepared using nmeauth.cls

Given the above, we limit the discussion here to homogeneous boundary conditions only, i.e. we consider problems with

$$\mathcal{C} = \left\{ \boldsymbol{u}(\boldsymbol{X},t) : \mathcal{B}^0 \to \mathbb{R}^3 \mid \boldsymbol{u}(\boldsymbol{X},t) = \boldsymbol{0} \ \text{ on } \ \partial^u \mathcal{B}^0 \right\} \ , \tag{29}$$

and

$$\mathcal{C}_h = \left\{ \boldsymbol{u}_h(\boldsymbol{X},t) \mid \boldsymbol{u}_h(\boldsymbol{X},t) = \boldsymbol{0} \ \text{ on } \ \partial^u \mathcal{B}_h^0 \right\} \ . \tag{30}$$

Hence, also (22) becomes

$$\widehat{\mathcal{C}}_h = \left\{ \widehat{\boldsymbol{u}}_h(\boldsymbol{X},t) \mid \widehat{\boldsymbol{u}}_h(\boldsymbol{X},t) = \boldsymbol{0} \ \text{ on } \ \partial^u \mathcal{B}_h^0 \right\} \ . \tag{31}$$

A discussion of general boundary value problems with inhomogeneous essential boundary conditions of type (2) is offered at the end of this section.

INCREMENT REPRESENTATION. So far, we have found a reduced representation of the configuration variable $\boldsymbol{u}$ (configuration space), which may be applied in Eq. (14). However, our ultimate goal is to reduce the dimension in the Newmark algorithm (20).

It is important to realize that the Newton-Raphson algorithm, which constitutes the equilibrium iteration in (20), is formulated in the tangent space to the configuration space $\mathcal{C}$, i.e. in the space of variations $\mathcal{V}$. Hence, we need to find a reduced representation for two spaces, $\widehat{\mathcal{C}}_h$ and $\widehat{\mathcal{V}}_h$ (the space of reduced variations). However, comparing (11) and (30) it is evident that for homogeneous boundary conditions $\mathcal{V}_h = \mathcal{C}_h$, and therefore also $\widehat{\mathcal{V}}_h = \widehat{\mathcal{C}}_h$.

NEWMARK IMPLICIT ALGORITHM IN THE REDUCED BASIS. The increment of displacement $\Delta\boldsymbol{u}^{(i)}$ in the i^{th} iteration is expanded into the Ritz basis of M functions $\boldsymbol{\phi}^j(\boldsymbol{X})$ as

$$\Delta\boldsymbol{u}^{(i)}(\boldsymbol{X}) = \sum_j^M \boldsymbol{\phi}^j(\boldsymbol{X}) \Delta p_j^{(i)} = \boldsymbol{\Phi}(\boldsymbol{X}) \Delta\boldsymbol{p}^{(i)} \ , \tag{32}$$

where we have introduced the matrix $\boldsymbol{\Phi}(\boldsymbol{X})$, constituted of the functions $\boldsymbol{\phi}^j(\boldsymbol{X})$ as columns. Note that the coefficients $\Delta p_j^{(i)}$ in (32) are just numbers, *not* functions of time. They express the contribution of the individual modes to the configuration correction generated by the current residual vector.

Using (32) for the variations $\boldsymbol{\eta}$ and increments $\Delta\boldsymbol{u}$ in the linearization of (19) leads to the reduced tangent. For simplicity, let us look at the transformation of the right hand side of Equation (15):

$$\sum_{I,J}^N \boldsymbol{\eta}_I \cdot \boldsymbol{K}_{IJ} \cdot \Delta\boldsymbol{u}_J \ .$$

Transformation (32) yields $\boldsymbol{\eta}_I = \boldsymbol{\Phi}\widetilde{\boldsymbol{\eta}}_I$ and $\Delta\boldsymbol{u}_J = \boldsymbol{\Phi}\Delta\boldsymbol{p}_J$, and the above expression is re-written in terms of the new variables as

$$\sum_{I,J}^N \boldsymbol{\eta}_I \cdot \boldsymbol{K}_{IJ} \cdot \Delta\boldsymbol{u}_J = \sum_{I,J}^N (\boldsymbol{\Phi}\widetilde{\boldsymbol{\eta}}_I) \cdot \boldsymbol{K}_{IJ} \cdot (\boldsymbol{\Phi}\Delta\boldsymbol{p}_J) = \sum_{I,J}^N \widetilde{\boldsymbol{\eta}}_I \cdot \boldsymbol{\Phi}^T \boldsymbol{K}_{IJ} \boldsymbol{\Phi} \cdot \Delta\boldsymbol{p}_J \ .$$

This procedure allows us to rewrite the expression for the displacement correction from algorithm (20),

$$\Delta\boldsymbol{u}^{(i)} = \boldsymbol{K}^{\mathrm{eff}(i)\,-1} \boldsymbol{R}^{(i)} \ ,$$

as

$$\Delta\boldsymbol{u}^{(i)} = \boldsymbol{\Phi}\Delta\boldsymbol{p}^{(i)} = \boldsymbol{\Phi} \left\{ \left(\boldsymbol{\Phi}^T \boldsymbol{K}^{\mathrm{eff}(i)} \boldsymbol{\Phi} \right)^{-1} \left[\boldsymbol{\Phi}^T \boldsymbol{R}^{(i)} \right] \right\} \ , \tag{33}$$

Copyright © 2000 John Wiley & Sons, Ltd.

Prepared using nmeauth.cls

where the order of evaluation is indicated by the parentheses. The reduced effective tangent stiffness matrix $\boldsymbol{\Phi}^T \boldsymbol{K}^{\mathrm{eff}(i)} \boldsymbol{\Phi}$ is an $M \times M$ matrix, which is assembled from transformed elementwise matrices $\boldsymbol{K}_e^{\mathrm{eff}(i)}$ using the standard assembly operator $\mathbf{A}$ (see for example Reference 37),

$$\boldsymbol{\Phi}^T \boldsymbol{K}^{\mathrm{eff}(i)} \boldsymbol{\Phi} = \mathop{\mathbf{A}}_{e=1}^{E} \boldsymbol{\Phi}_e^T \boldsymbol{K}_e^{\mathrm{eff}(i)} \boldsymbol{\Phi}_e \ . \tag{34}$$

The matrices $\boldsymbol{\Phi}_e$ are extracted from the appropriate rows of the matrix $\boldsymbol{\Phi}$, and collect the modal amplitudes for the nodes of the element e. Favorable computational cost and storage requirements are obtained by assembling the reduced element matrices as opposed to reducing the full assembled matrix $\boldsymbol{K}^{\mathrm{eff}(i)}$ (operation count of $O(N)$ vs. $O(N^2)$ and negligible storage for the $M \times M$ matrix).

The overall Newmark algorithm for the reduced FE model is summarized as (the operations which experienced any changes are labeled on the left with boxed text)

$$\begin{aligned}
& i \leftarrow 0 \\
& \left.\begin{aligned}
\boldsymbol{u}_{t+\Delta t}^{(i)} &= \boldsymbol{u}_t, \\
\boldsymbol{a}_{t+\Delta t}^{(i)} &= -\frac{1}{\beta \Delta t} \boldsymbol{v}_t + \left(1 - \frac{1}{2\beta}\right) \boldsymbol{a}_t, \\
\boldsymbol{v}_{t+\Delta t}^{(i)} &= \boldsymbol{v}_t + \Delta t \left[(1-\gamma)\, \boldsymbol{a}_t + \gamma \boldsymbol{a}_{t+\Delta t}^{(i)}\right]
\end{aligned}\right\} && \text{predictor} \\
& i \leftarrow i + 1 && \text{next iteration} \\
& \boldsymbol{\Phi}^T \boldsymbol{K}^{\mathrm{eff}(i)} \boldsymbol{\Phi} = \mathop{\mathbf{A}}_{e=1}^{E} \boldsymbol{\Phi}_e^T \left(\frac{1}{\beta \Delta t^2} \boldsymbol{M}_e + \boldsymbol{K}_e^{\mathrm{m}(i)} + \boldsymbol{K}_e^{\sigma(i)} \right) \boldsymbol{\Phi}_e && \boxed{\text{eff. stiffness}} \\
& \boldsymbol{R}^{(i)} = \boldsymbol{M} \boldsymbol{a}_{t+\Delta t}^{(i)} - \boldsymbol{f}_{t+\Delta t}^{\mathrm{ext}(i)} + \boldsymbol{f}_{t+\Delta t}^{\mathrm{int}(i)} && \text{residual} \\
& \Delta \boldsymbol{u}^{(i)} = \boldsymbol{\Phi} \left(\boldsymbol{\Phi}^T \boldsymbol{K}^{\mathrm{eff}(i)} \boldsymbol{\Phi} \right)^{-1} \boldsymbol{\Phi}^T \boldsymbol{R}^{(i)} && \boxed{\text{displ. increment}} \\
& \left.\begin{aligned}
\boldsymbol{u}_{t+\Delta t}^{(i)} &= \boldsymbol{u}_{t+\Delta t}^{(i-1)} + \Delta \boldsymbol{u}^{(i)} \\
\boldsymbol{v}_{t+\Delta t}^{(i)} &= \boldsymbol{v}_{t+\Delta t}^{(i-1)} + \frac{\gamma}{\beta \Delta t} \Delta \boldsymbol{u}^{(i)} \\
\boldsymbol{a}_{t+\Delta t}^{(i)} &= \boldsymbol{a}_{t+\Delta t}^{(i-1)} + \frac{1}{\beta \Delta t^2} \Delta \boldsymbol{u}^{(i)}
\end{aligned}\right\} && \text{corrector}
\end{aligned} \tag{35}$$

If $||\boldsymbol{R}^{(i)}|| > \epsilon ||\boldsymbol{R}^{(0)}||$ repeat for next iteration;

else $t \leftarrow t + \Delta t$ and go to the top.

Asymptotic Costs. The solution costs for the full and reduced-dimension models are summarized in Table II (N is the number of nodes, and M is the number of modes in the Ritz basis). The exact form of the function $s(N)$ depends on the solver used, on the sparsity of the effective tangent stiffness matrix etc. For instance, sparse-matrix iterative solvers typically incur $O(N)$ cost per iteration, and the number of iterations itself might depend on the dimension of the matrix.

The asymptotic cost estimates of Table II clearly indicate potential savings if the number of modes M grows much more slowly than N, or if M is bounded from above. While it may not be easy to come up with some general theoretical statements regarding M, numerical experiments indicate that the dependence of M on N is very weak indeed.

Inhomogeneous Boundary Conditions. It would seem that limiting our model-dimension reduction approach to the case of homogeneous boundary condition (BC) is overly restricting in practical applications. However, in a number of important applications a coordinate frame may be chosen which converts problems with inhomogeneous boundary condition (BC) (Equation (10)) into the homogeneous BC case. One example is found in earthquake engineering: the synchronous seismic base excitation. It is common practice to formulate the equations of motion in the accelerated frame attached to the base, and include the excitation via an inertial load term. Other approaches to the

Copyright © 2000 John Wiley & Sons, Ltd.

Prepared using nmeauth.cls

Operation	Full system	Reduced system
Predictor	$O(N)$	$O(N)$
Force assembly	$O(N)$	$O(NM)$
Tangent assembly	$O(N)$	$O(NM^2)$
Solve for displ. incr.	$O[s(N)]$	$O(M^3)$
Configuration update	$O(N)$	$O(NM)$

Table II. Asymptotic cost of the Newmark implicit algorithm operations

solution of the general case of inhomogeneous BC include penalty methods or methods of Lagrangian multipliers, which convert an essential BC into a natural BC. Therefore, it is our opinion that the restriction to homogeneous BC does not detract from the practicality of our approach.

Other classes of mechanical systems with constraints, for instance incompressibility, have been discussed in Reference 23, which also deals with more general configuration manifolds.

3. MODEL DIMENSION REDUCTION FOR EXPLICIT INTEGRATION

Central difference discretization of the equations of motion is widely used in solid mechanics, for instance in the form of the explicit Newmark beta method ($\beta = 0$), whose algorithmic equations are

$$\begin{aligned} \boldsymbol{v}_t &= \boldsymbol{v}_{t-\Delta t} + \frac{\Delta t}{2}\left(\boldsymbol{a}_t + \boldsymbol{a}_{t-\Delta t}\right) \\ \boldsymbol{u}_{t+\Delta t} &= \boldsymbol{u}_t + \Delta t \boldsymbol{v}_t + \frac{\Delta t^2}{2}\boldsymbol{a}_t \\ \boldsymbol{M}\boldsymbol{a}_{t+\Delta t} &= \boldsymbol{f}^{\text{ext}}_{t+\Delta t} - \boldsymbol{f}^{int}_{t+\Delta t} \end{aligned} \tag{36}$$

where $\boldsymbol{M}$ is a time-independent, diagonal mass matrix; $\boldsymbol{u}_\tau$, $\boldsymbol{v}_\tau$, $\boldsymbol{a}_\tau$ are the vectors of displacements, velocities, and accelerations, and $\boldsymbol{f}^{\text{ext}}_\tau$ and $\boldsymbol{f}^{\text{int}}_\tau$ are the external and internal forces, all at time τ.

Implementation of Explicit Dynamics in the Reduced Basis. Reduction of the last equation in (36) analogous to that of equation (33) yields

$$\boldsymbol{a}_{t+\Delta t} = \boldsymbol{\Phi}\left(\boldsymbol{\Phi}^T\boldsymbol{M}\boldsymbol{\Phi}\right)^{-1}\boldsymbol{\Phi}^T\widehat{\boldsymbol{f}}_{t+\Delta t}\ . \tag{37}$$

where $\widehat{\boldsymbol{f}}_{t+\Delta t} = \boldsymbol{f}^{\text{ext}}_{t+\Delta t} - \boldsymbol{f}^{int}_{t+\Delta t}$. The temptation to precompute the matrix $\boldsymbol{\Phi}\left(\boldsymbol{\Phi}^T\boldsymbol{M}\boldsymbol{\Phi}\right)^{-1}\boldsymbol{\Phi}^T$ (both $\boldsymbol{M}$ and $\boldsymbol{\Phi}$ are time-independent matrices), and to solve for the accelerations by multiplying with this precomputed matrix, should be resisted: the cost would grow asymptotically as $O(N^2)$, not to mention the need to store a big dense matrix. The two alternative orders of evaluation are

$$\boldsymbol{\Phi}\left[\left(\boldsymbol{\Phi}^T\boldsymbol{M}\boldsymbol{\Phi}\right)^{-1}\left(\boldsymbol{\Phi}^T\widehat{\boldsymbol{f}}_{t+\Delta t}\right)\right]\ , \tag{38}$$

where the part precomputed before the time stepping starts is the matrix $\left(\boldsymbol{\Phi}^T\boldsymbol{M}\boldsymbol{\Phi}\right)^{-1}$, and

$$\boldsymbol{\Phi}\left\{\left[\left(\boldsymbol{\Phi}^T\boldsymbol{M}\boldsymbol{\Phi}\right)^{-1}\boldsymbol{\Phi}^T\right]\widehat{\boldsymbol{f}}_{t+\Delta t}\right\}\ , \tag{39}$$

where the precomputed matrix is $\left(\boldsymbol{\Phi}^T\boldsymbol{M}\boldsymbol{\Phi}\right)^{-1}\boldsymbol{\Phi}^T$. The asymptotic cost of both (38) and (39) is $O(MN)$. We have adopted equation (38) because of lower storage requirements.

Copyright © 2000 John Wiley & Sons, Ltd.

Prepared using nmeauth.cls

Asymptotic Costs. The solution costs for the full and reduced-dimension models are summarized in Table III, where N is the number of nodes, and M is the number of modes in the Ritz basis. While Table III seems to indicate that nothing is in fact gained by using the reduced basis (the operations per time step cost more, not less), there is one important aspect which "saves the day," and that is the stable time step magnitude: Using global modes in general increases the stable time step, and since the transformations into and from the reduced basis are relatively inexpensive, the longer stable time step projects almost fully into decreased run-times.

Operation	Full system	Reduced system
Force assembly	$O(N)$	$O(N)$
Solve for accelerations	$O(N)$	$O(NM)$
Configuration update	$O(N)$	$O(NM)$

Table III. Asymptotic cost of the central difference algorithm operations

4. EMPIRICAL EIGENVECTOR BASIS

Up to now, the issue of the choice of the basis vectors to be used in the incremental Ritz algorithm was intentionally left unresolved. In this section, a particular set of generalized coordinates is proposed, the ***empirical eigenvectors*** (EE), which is based on the statistical view of the response of the full finite element (FE) model.

Empirical eigenvectors are obtained by a procedure which goes back at least to the papers of Pearson [33], and Schmidt [36], and which (re)appears under a multitude of names as Karhunen-Loève expansion [20, 25], principal component analysis [13], empirical orthogonal eigenfunctions [26], factor analysis [11], proper orthogonal decomposition [27], and total least squares [10]. The singular value decomposition algorithm [10] is the key to the understanding of these methods. Applications of this approach are found in many engineering and scientific disciplines; consult, for instance, References 41 and 12. The only application of EE's to solid mechanics known to the authors is a conversion a finite difference model of torsional vibrations of drill-strings to a lower-dimensional analytical dynamic system [22].

Use of EE's in Solid Dynamics. The exposition of Reference 8 is adapted here to FE models. Consider a solid body subjected to some dynamic loads during a time interval $\mathcal{I}$. Mark arbitrary N points on the surface of the body and/or in its interior, and record the positions of these N points at S instants during the interval $\mathcal{I}$. Collect the observations into an ensemble of $3N$-dimensional vectors, $\boldsymbol{u}^j \in \mathbb{R}^{3N}, j = 1, \ldots, S$ (there are three displacement components for each of the N points). Center the ensemble by subtracting its average, $\bar{\boldsymbol{u}}$,

$$\bar{\boldsymbol{u}} = \langle \boldsymbol{u}^i \rangle = \frac{1}{S} \sum_{i=1}^{S} \boldsymbol{u}^i \ , \tag{40}$$

and collect the centered vectors as columns of the matrix $\boldsymbol{U}$

$$\underset{N\times S}{\boldsymbol{U}} = \left[\bar{\boldsymbol{u}}^1, \bar{\boldsymbol{u}}^2, \ldots, \bar{\boldsymbol{u}}^S \right] \ . \tag{41}$$

where

$$\bar{\boldsymbol{u}}^j = \boldsymbol{u}^j - \bar{\boldsymbol{u}} \ .$$

Copyright © 2000 John Wiley & Sons, Ltd.

Prepared using nmeauth.cls

If an approximation to the vector ensemble $\boldsymbol{u}^j$ is sought in the form

$$\widetilde{\boldsymbol{u}} = \boldsymbol{v}_0 + \sum_{i=1}^{M} w_i(\boldsymbol{u} - \bar{\boldsymbol{u}})\boldsymbol{v}^i \tag{42}$$

with $M < N$, the expectation

$$E\left(\|\boldsymbol{u} - (\boldsymbol{v}_0 + \sum_{i=1}^{M} w_i(\boldsymbol{u} - \bar{\boldsymbol{u}})\boldsymbol{v}^i)\|^2\right) \tag{43}$$

is minimized by $\boldsymbol{v}_0 = \bar{\boldsymbol{u}}$, $\boldsymbol{v}^i = \boldsymbol{\phi}^i$, and $w_i(\boldsymbol{x}) = \boldsymbol{x}^T \cdot \boldsymbol{\phi}^i$, where $\boldsymbol{\phi}^i$ are the orthonormal eigenvectors of the covariance matrix

$$\boldsymbol{C}_d = \frac{1}{M}\boldsymbol{U}\boldsymbol{U}^T \tag{44}$$

corresponding to the eigenvalues $\lambda_1 \geq \lambda_2 \geq \ldots \geq \lambda_N$. (See Reference [6] for a proof.) In other words,

$$\widetilde{\boldsymbol{u}} = \bar{\boldsymbol{u}} + \sum_{i=1}^{M} \left[(\boldsymbol{u} - \bar{\boldsymbol{u}})^T \cdot \boldsymbol{\phi}^i\right] \boldsymbol{\phi}^i \tag{45}$$

is the best M-dimensional linear approximation to $\boldsymbol{u}$ in the quadratic mean. The approximation error is

$$E\left(||\boldsymbol{u} - \widetilde{\boldsymbol{u}}||^2\right) = \lambda_{M+1} + \ldots + \lambda_N \tag{46}$$

If the number of samples S is smaller than $3N$, the EE's may be computed advantageously by the *method of snapshots* [38–40]. The sample covariance matrix $\boldsymbol{C}_s$ is constructed as

$$\boldsymbol{C}_s = \frac{1}{M}\boldsymbol{U}^T\boldsymbol{U} \ . \tag{47}$$

The non-zero spectra of $\boldsymbol{C}_s$ and $\boldsymbol{C}_d$ are the same, and the eigenvectors of $\boldsymbol{C}_d$ corresponding to the non-zero eigenvalues are recovered by the procedure described in Reference [12].

Application to FEM Model Reduction. The above recipe is directly applied to finite element (FE) models by collecting displacements at all FE nodes. The EE's of the ensemble covariance matrix are then used in the incremental Ritz algorithm. Given current lack of proper a priori error estimation, the number of basis vectors required for given accuracy is found by trial and error.

The EE's are the *optimal* generalized coordinates for a given FE model and given boundary and initial conditions. However, using the EE's computed for a particular FE model for a similar model as a near-optimal basis is feasible when the response of the two full FE models is not drastically different. One example of this is given in the section on numerical tests.

The sampled displacements may be obtained either from experiments or from computations with the full FE model. If the EE basis can be used many times over, for example to explore a large design space, or in the design of a non-linear controller, the cost of the computation of the EE's from the full model simulation may be amortized.

Alternate interpretation of the EE's. Assume that each centered sample in the configuration space, $\bar{\boldsymbol{u}}^j$, represents a particle of unit mass. The moment of inertia of the ensemble $\bar{\boldsymbol{u}}^j, j = 1, \ldots, S$

$$\boldsymbol{I} = \left(\sum_i \|\bar{\boldsymbol{u}}^i\|^2\right)\mathbf{1} - \boldsymbol{U}\boldsymbol{U}^T \ = I_R\mathbf{1} - \boldsymbol{U}\boldsymbol{U}^T, \tag{48}$$

where

$$I_R = \sum_i \|\bar{\boldsymbol{u}}^i\|^2$$

Copyright © 2000 John Wiley & Sons, Ltd.

Prepared using nmeauth.cls

is the polar moment of inertia, $\|\bar{\boldsymbol{u}}^i\|^2 = \bar{\boldsymbol{u}}^i \cdot \bar{\boldsymbol{u}}^i$, and $\boldsymbol{U}$ was defined in (41). An eigenvalue problem is now formulated for the moment of inertia $\boldsymbol{I}$ as

$$\boldsymbol{I}\boldsymbol{v} = \mu\boldsymbol{v} = \left(I_R\mathbf{1} - \boldsymbol{U}\boldsymbol{U}^T\right)\boldsymbol{v} = \mu\boldsymbol{v} \ , \tag{49}$$

and it immediately follows that

$$\boldsymbol{U}\boldsymbol{U}^T\boldsymbol{v} = (I_R - \mu)\,\boldsymbol{v} \ . \tag{50}$$

However, since the eigenvalue problem for the covariance matrix $\boldsymbol{C}_d$ is

$$\boldsymbol{C}_d\boldsymbol{w} = \lambda\boldsymbol{w} = \frac{1}{M}\boldsymbol{U}\boldsymbol{U}^T\boldsymbol{w} \ ,$$

we arrive at the result

$$\boldsymbol{w} = \boldsymbol{v} \tag{51}$$

$$\lambda = \frac{I_R - \mu}{M} \tag{52}$$

In words, the principal directions of the covariance matrix $\boldsymbol{C}_d$ correspond to the principal directions of the moment of inertia $\boldsymbol{I}$, and there is a one to one correspondence between the eigenvalues. The directions that are selected for the optimal representation from the eigenproblem (49) are such that the moment of inertia of the samples about the eigenvector is as small as possible.

5. ERROR ESTIMATION AND ADAPTIVITY

The discussion in this section is limited to the model dimension reduction for the implicit Newmark integration algorithm. Furthermore, the effects of deterministic chaos are excluded from consideration by limiting the discussion to relatively short-term dynamics.

Error Estimation. Assume that the a posteriori error of the full finite element model can be determined. Then, the error in the response of the reduced-dimension model may be estimated, provided the difference between the response of the full and reduced models can be bounded. The source of the difference in the response of the full and reduced models in our incremental Ritz algorithm is the expansion of the incremental displacement in a reduced number of modes. In other words, the failure of the reduced basis of M terms to represent the incremental displacements of the full FE model prevents the equilibrium iteration from reducing the force residual to a zero vector.

The effects of basis truncation are more or less well understood in problems of linear vibration [2, 3, 14, 18, 21, 46], but do not appear to have been seriously studied for non-linear dynamic deformation problems. Attempts to quantify the truncation error have so far been directed at the usual approach, that is the time integration of the modal model. Thus, for instance, Idelsohn and Cardona [15] monitored the magnitude of the error in the residual force, and recomputed the reduced basis when the normalized error exceeded an arbitrarily set tolerance. Joo, Wilson and Leger [18] suggested truncation criteria based on the error in the projection of the applied load (or alternatively, the residual force) onto the Ritz vectors, and Chang and Engblom [5] used so-called mode participation factors to guide the generation of the reduced basis. However, the most important piece of information that is still missing is how to link the residual imbalance to other error measures, most importantly to those relevant to the applicability of the model reduction algorithm in applications: Among others, energy dissipation rate, kinetic energy (global measures); and displacement, strain, force, stress, damage or other material history variable (local measures).

To fix ideas, consider the representation of the residual force vector in the reduced basis

$$\widetilde{\boldsymbol{R}} = \sum_j \left[(\boldsymbol{\phi}^j)^T\boldsymbol{R}\right]\boldsymbol{\phi}^j \tag{53}$$

Copyright © 2000 John Wiley & Sons, Ltd.

Prepared using nmeauth.cls

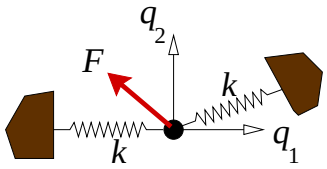

Figure 1. Concentrated mass supported by two springs with elastic constant k in a plane. Forcing: $F_i(t) = \widehat{F}_i \cos(\omega_i t + \psi_i)$, $\omega_1 \neq \omega_2$, $\psi_1 \neq \psi_2$. Displacements are on the order of one fifth of the length of the springs.

where orthonormality of modes has been assumed. Now note that the (convergent) equilibrium iteration in the reduced basis works towards decreasing $|(\boldsymbol{\phi}^j)^T \boldsymbol{R}|$ to zero. This occurs for either (i) $\|\boldsymbol{R}\| \to 0$, or (ii) $|(\boldsymbol{\phi}^j)^T \boldsymbol{R}| \to 0$ for each j. The latter possibility is just an expression of the orthogonality of the basis vectors to the residual $\boldsymbol{R}$. Therefore, if $\boldsymbol{R}$ can be expressed fully in the basis $\boldsymbol{\phi}^j$, convergence in the reduced basis implies $\|\boldsymbol{R}\| \to 0$; on the other hand, failure to reproduce $\boldsymbol{R}$ by $\widetilde{\boldsymbol{R}}$ indicates that $\|\boldsymbol{R}\|$ cannot in general be made to approach the zero vector during the equilibrium iteration in the reduced basis. Define the normalized residual projection error, for example, as

$$\epsilon_R = \frac{|\boldsymbol{R}^T(\boldsymbol{R} - \widetilde{\boldsymbol{R}})|}{\boldsymbol{R}^T \boldsymbol{R}} \tag{54}$$

To relate ϵ_R to some error measure of practical interest, for instance the L_2-norm of the difference in kinetic energy, does not seem feasible without knowing the importance of the irremovable residual force compared to the external loads and inertial forces acting on the FE model. This aspect of the error estimation is currently under investigation.

Adaptivity. Provided truncation error can be related to some practical measures of error, the issue of adaptive reduced basis control can be attacked. In other words, the *truncation error* may be adaptively controlled by enhancing the approximation basis, or by adopting a completely different basis (if necessary, at any equilibrium iteration). Selection of a few modes from a larger set by the magnitude of the participation factor $(\boldsymbol{\phi}^j)^T \boldsymbol{R}$, or from an explicit Euler step or from the various forms of the Newmark predictor are currently being considered, among other options.

Convergence Analyses. An area of application which is currently being explored are convergence studies, where the EE basis obtained for a coarse model is applied after intelligent re-interpolation to a refined model, and the response of the refined model is obtained by time integration with the incremental Ritz procedure.

6. COMPARISON WITH THE LINEARIZATION-BASED APPROACH

The difference between our approach and the traditional linearization-based approach may be illustrated very well on the following example of a two-degree-of-freedom mechanical system; see Figure 1. The solid curve represents the evolution of the full mechanical system in time ("full" means with both degrees of freedom, q_1 and q_2). If a linearization-based reduced model (with just a single degree of freedom) is constructed at point A, the point in the q_1, q_2 plane representing the configuration of the system is restricted to move along a line given by the arrow at point A, and passing through A. This one-mode reduced model is a very good approximation of the full model in the immediate vicinity of A, but becomes progressively worse as the solutions diverge from point A. Evidently, basing the reduced model on the tangent direction at point B would lead to even worse accuracy away from the linearization point.

In contrast, the statistics-based (global) basis is not taylored to the response at any particular point on the curve, but rather it fits the elongated shape of the curve in a statistical sense. As explained in Section 4, intuitive insight follows from viewing the data points as massive particles in the configuration

Copyright © 2000 John Wiley & Sons, Ltd.

Prepared using nmeauth.cls

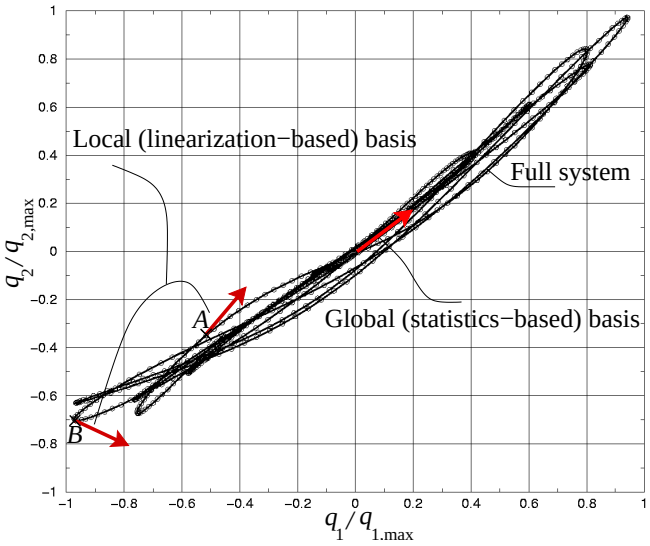

Figure 2. Comparison of local (linearization-based) reduced basis and global (statistics-based) reduced basis for a two-degree-of-freedom mechanical system.

space: the optimal modes (directions) are those which minimize the moment of inertia of the particles about that direction as axis of rotation.

It is evident from the above, that the reduced model based on a local expansion of the response is likely to require frequent change or update of the basis. In addition to being costly, any change to the basis is also precarious, for at least two reasons. Firstly, removal or addition of a basis function amounts to the introduction of a time-dependent constraint into the formulation of the mechanical problem. That means that the original characteristics of the solution (conservation of energy, for example) may be lost by the change in the basis during the time stepping. Secondly, if the time stepping is done in terms of the modal coefficients (which was the rule in the existing literature [5, 16, 30, 32, 34], Tao and Ramm [43] being the only exception), the change in the basis needs to be accompanied by a projection of the current solution into the new basis as the initial state for the new modal coefficients. This procedure introduces an uncontrolled imbalance into the equations of motion, which may adversely affect the accuracy of the subsequent solution. Moreover, this is a cumulative effect, which affects all solutions later in time, directly by the force imbalance, and indirectly by deteriorating quality of subsequent tangent-response bases.

The distinction between the configuration and variation spaces does not appear to have been made in the literature. This might be the result of the implicit assumption of homogeneous boundary conditions. Thus, either the need for two reduced bases (for the configuration and variation spaces) had been overlooked, or unacknowledged (unknowing, perhaps) use had been made of the identification of the two spaces for the case of homogeneous boundary condition.

7. EXAMPLES

The complete specification of the mechanical problems referred to in this Section is available from the web site [29].

Empirical eigenvectors are used exclusively in the incremental-Ritz reduced models of this section.

Copyright © 2000 John Wiley & Sons, Ltd.

Prepared using nmeauth.cls

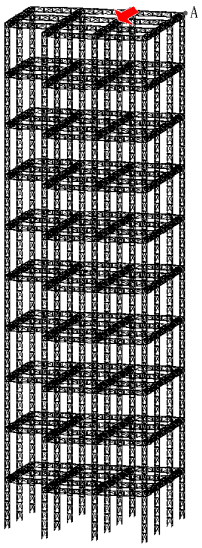

Figure 3. Tall truss frame structure.

The set of basis vectors is not changed during the simulations.

TALL TRUSS FRAME. A tall frame composed of truss beams and columns is subjected to gravity loads combined with a horizontal force with a triangular pulse time dependence. The material is linear elastic, roughly corresponding to construction steel. The finite element (FE) model consists of 7,180 nodes (21,540 degrees of freedom, of which 180 at the base are constrained to zero), and 27,540 rod elements. The horizontal load is applied as indicated by the arrow, and the displacement is monitored in the upper-right corner (point A in Figure 3). (The amplitude of the horizontal motion is roughly 2/3 of the column spacing.)

Figure 4 shows the response of the full FE model at point A for the given horizontal load, and for three magnitudes of the vertical (gravity) load, $1/2g$, g, and $2g$. As predicted by the well-known engineering P-Δ theory, the apparent period increases with larger vertical load, and decreases with smaller load. The amplitude is also affected.

The response of the full FE model has been obtained for the full gravity load g by an implicit integration with full Newton-Raphson equilibrium iteration, and with a time step 500 time longer than the largest stable explicit time step. The empirical eigenfunctions have been computed by the snapshot method from 150 samples uniformly spaced in the interval $0 \leq t \leq 1.5$ seconds. Figures 5 and 6 show the deflection in the direction of the horizontal force at point A, and the kinetic energy respectively, for the full model compared with various-order reduced models. Nine modes provide decent approximation, especially in the kinetic energy, and with 15 modes even the deflections are virtually indistinguishable from those computed with the full system.

The empirical basis computed for the vertical load $g = 1$ is no longer optimal for models loaded by gravity loads $g = 1/2$ or $g = 2$. However, since the response of the full models has a similar character, it might be intuitively expected that even a non-optimal empirical basis will capture the dynamics well. To verify that this is the case, the response for $g = 1/2$ and $g = 2$ has been computed with reduced-dimension models based on the EE's obtained for $g = 1$. Figures 7 (for $g = 1/2$) and 8 (for $g = 2$) demonstrate convincingly the near-optimality of the EE basis: results for the reduced models with the same number of modes are of quality similar to that of Figure 5.

TIMING COMPARISONS FOR THE TALL FRAME SIMULATION. An implicit Newmark simulation with full Newton-Raphson iteration of equilibrium, run with a time step 500 times longer than the largest

Copyright © 2000 John Wiley & Sons, Ltd.

Prepared using nmeauth.cls

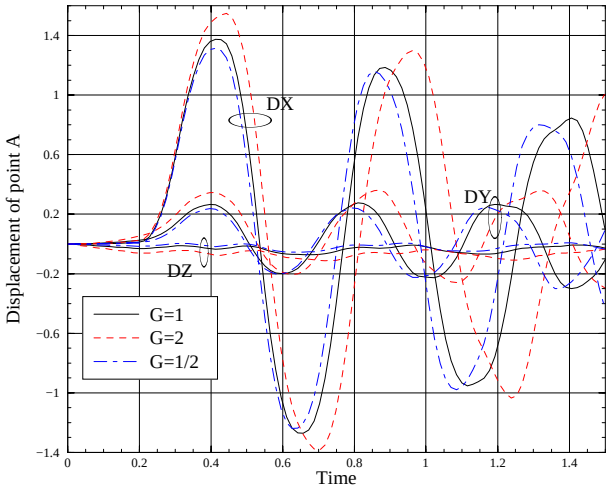

Figure 4. Response of the full system for different magnitudes of the vertical load.

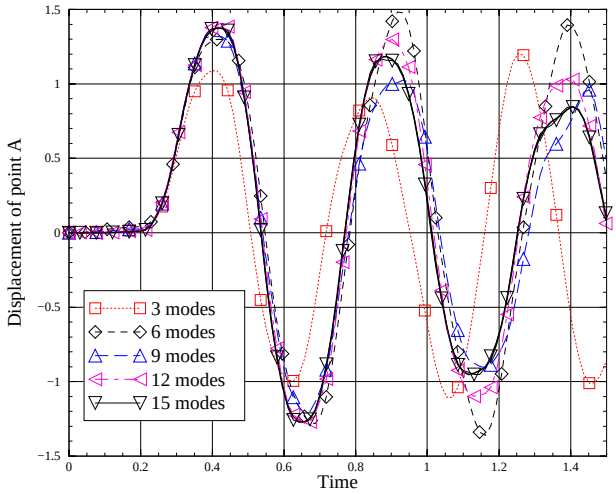

Figure 5. Tall truss frame. Displacement of point A in the direction of the horizontal load for $g = 1$.

stable explicit time step, takes 8,540 seconds*. A single step of the Newton-Raphson iteration in the implicit simulation requires: residual force assembly 0.33 seconds, effective tangent stiffness assembly 1.50 seconds, solve 26.86 seconds (sparse LU decomposition), and the configuration predictor and corrector take roughly 0.02 seconds each. An explicit simulation consumes 14,700 seconds. Finally,

*All timings in this paper given as wall-clock measurements on an 225 MHz SGI Octane workstation with R10K processor, 128 MB of memory, and 32 KB instruction and data caches, and 1 MB secondary cache.

Copyright © 2000 John Wiley & Sons, Ltd.

Prepared using nmeauth.cls

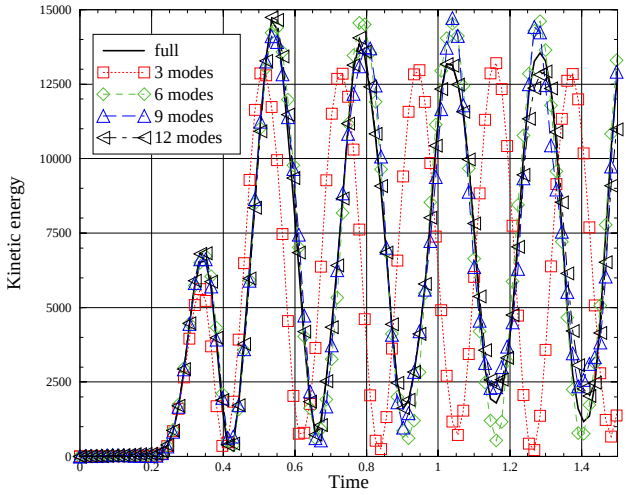

Figure 6. Tall truss frame. Kinetic energy for $g = 1$.

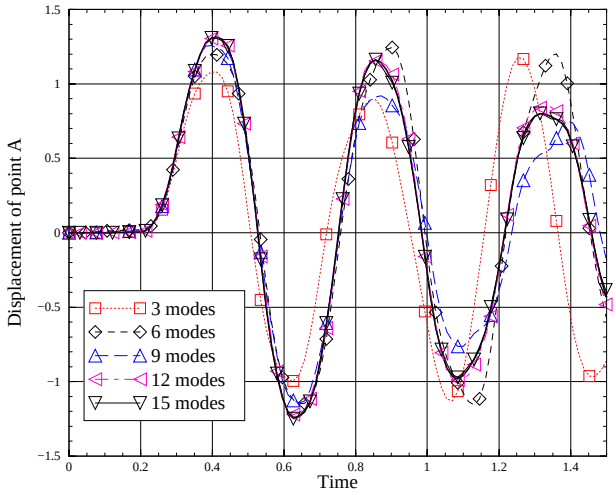

Figure 7. Tall truss frame. Displacement of point A in the direction of the horizontal load for $g = 1/2$.

simulations with the reduced model require 6% of the implicit simulation run time for 3 modes, 7.5% for 6 modes, 10.5% for 9 modes, 13.3% for 12 modes and 16.9% for 15 modes. Therefore, even with the costliest reduced model the run time is reduced by a factor of six with respect to the full implicit model.

FRAME UNDER BODY-LOAD PULSE. A frame composed of straight square cross-section beams is clamped at one end, and a pulse of body load is applied in the vertical direction. The material is hyperelastic of the St.Venant-Kirchhoff type. Three FE models have been used, the coarsest with 41 hexahedral 8-noded elements ($h = 1$), and the finer ones obtained by tri-section of the elements on the previous level ($h = 1/2$ with 168 elements, and $h = 1/4$ with 1,344 elements). The frame experiences

Copyright © 2000 John Wiley & Sons, Ltd.

Prepared using nmeauth.cls

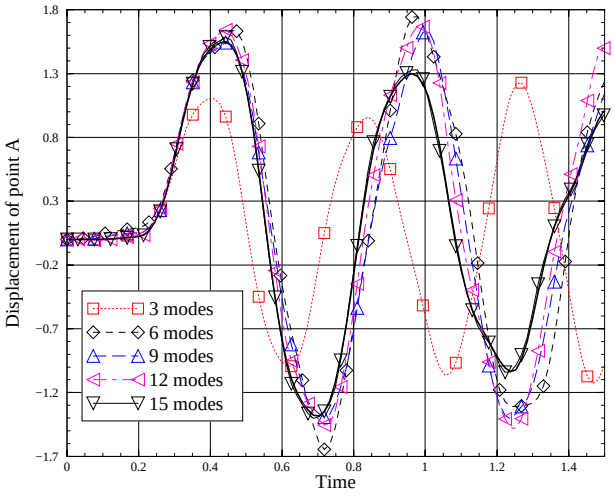

Figure 8. Tall truss frame. Displacement of point A in the direction of the horizontal load for $g = 2$.

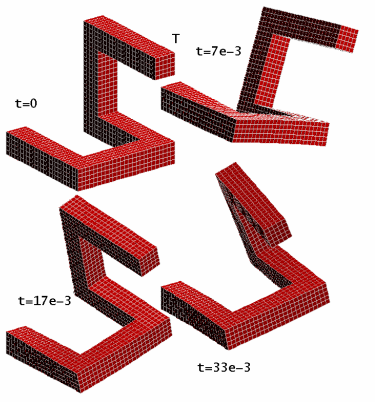

Figure 9. Selected shapes of the spatial frame during the simulation (FE model $h = 1/4$).

large displacements with moderate strains; Figure 9 shows some of the deformed shapes of the frame, and Figure 10 records the variation of the kinetic energy for the three full FE models.

The empirical basis has been computed from 140 snapshots uniformly distributed in the interval $\mathcal{I} = 0 \leq t \leq 0.01$ seconds. The difference in the response of the full FE model and its reduced version was measured in the kinetic energy (K_{full} is the kinetic energy computed with the full model, and K_{red} is the kinetic energy computed with the reduced model)

$$\epsilon_K = \frac{\int_{\mathcal{I}} |K_{full} - K_{red}| \, \mathrm{d}t}{\int_{\mathcal{I}} K_{full} \, \mathrm{d}t} \, ,$$

and the results are summarized in Figure 11: The error in kinetic energy ϵ_K is plotted on a logarithmic scale versus the number of modes. Figure 12 gives an indication of the accuracy of other quantities of possible interest, in this case vertical displacement of the tip. The response for $M = 30$ is visually

Copyright © 2000 John Wiley & Sons, Ltd.

Prepared using nmeauth.cls

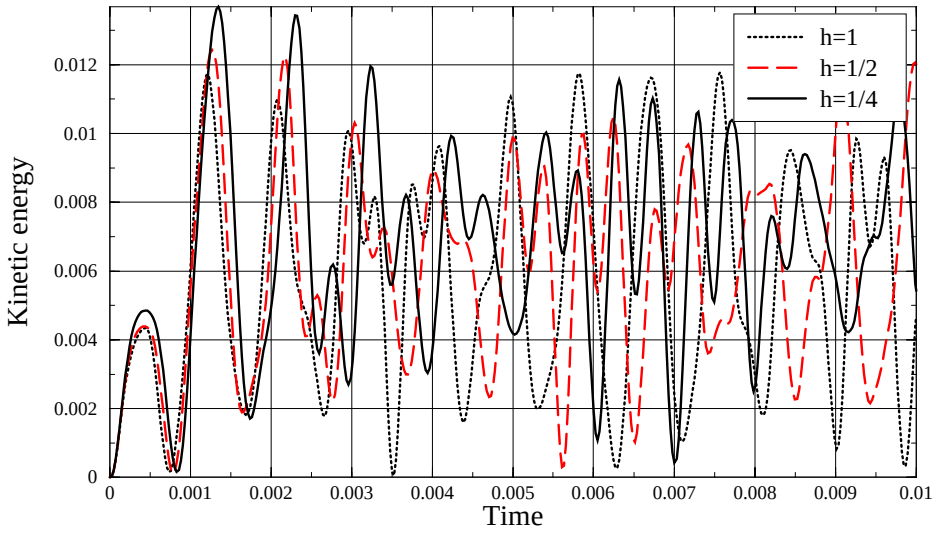

Figure 10. Spatial frame. Kinetic energy computed with full FE models.

indistinguishable from the response of the full model, and even for $M = 20$ the displacement agrees well with the full model results in the initial stages.

As apparent in Figure 10, there are substantial point-wise differences in the kinetic energy for the three FE models, but the overall variations in the three curves are comparable (amplitude, apparent period). That is a strong indication that the response could be perhaps described with about the same number of modes (basis functions), and indeed, results obtained with the reduced models confirm this conjecture. Given an error tolerance, for instance $\epsilon_K = 0.01$, the number of modes needed grows from 26 ($h = 1$) to 30 ($h = 1/4$), which is a 15% increase, while the number of degrees of freedom of the full FE models increases roughly 24 times between $h = 1$ and $h = 1/4$. Hence, the conclusion may be drawn that the number of Ritz modes grows much more slowly than the number of degrees of freedom of a full FE model, which is a key to the success of the reduction technique.

Notched Beam. A notched copper beam, supported at both ends, is loaded by a force pulse just above the notch which simulates the impact of a mass; see Figure 13. The beam deforms under this load inelastically; compare with Figure 14 demonstrating the relatively large deflections on the FE mesh. The material model is rate-independent J_2 elastoplasticity with kinematic hardening. The full FE model is comprised of 4,788 quadratic tetrahedral elements and 5,996 nodes. The time evolution is integrated in time by the explicit version of the Newmark algorithm.

Figure 15 shows the vertical deflection and the evolution of the equivalent plastic strain at the notch tip. The reduced models are based on 3 and 6 modes respectively. It is evident that even with the coarsest reduced model the response of the beam is reproduced surprisingly well, and the curves for 6 modes can be hardly distinguished from the full-model results. Simulation time for the 6-mode reduced model decreases to one ninth (1/9) of the full-model run time due to an increase in the stable time step.

CONCLUSIONS AND FUTURE DIRECTIONS

We have shown how both the explicit and implicit Newmark time stepping algorithms, which are commonly used with non-linear finite element (FE) models in solid and structural dynamics, can

Copyright © 2000 John Wiley & Sons, Ltd.

Prepared using nmeauth.cls

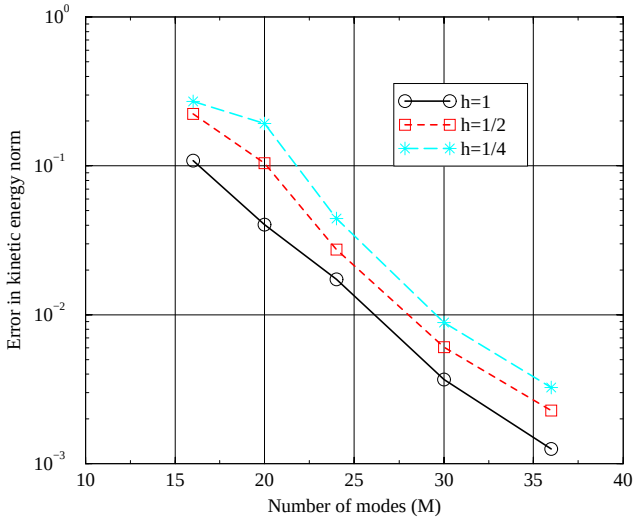

Figure 11. Spatial frame. Convergence in the kinetic energy.

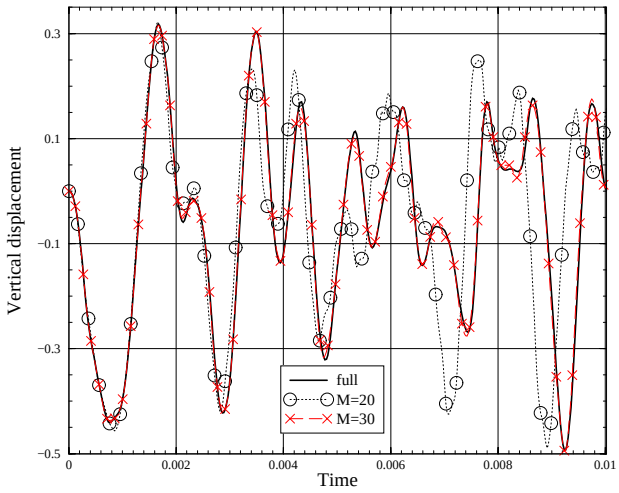

Figure 12. Vertical displacement of point T for $h = 1/4$. Full and reduced models.

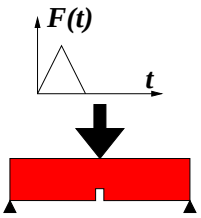

Figure 13. Elastoplastic deformation of notched beam. Problem setup.

Copyright © 2000 John Wiley & Sons, Ltd.

Prepared using nmeauth.cls

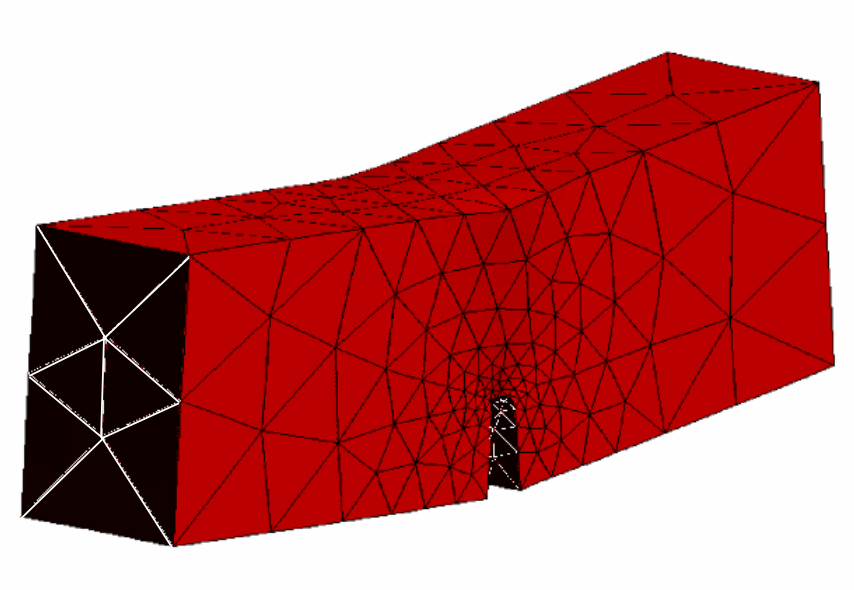

Figure 14. Elastoplastic deformation of notched beam. Deformed mesh at the end of the simulation. Actual scale.

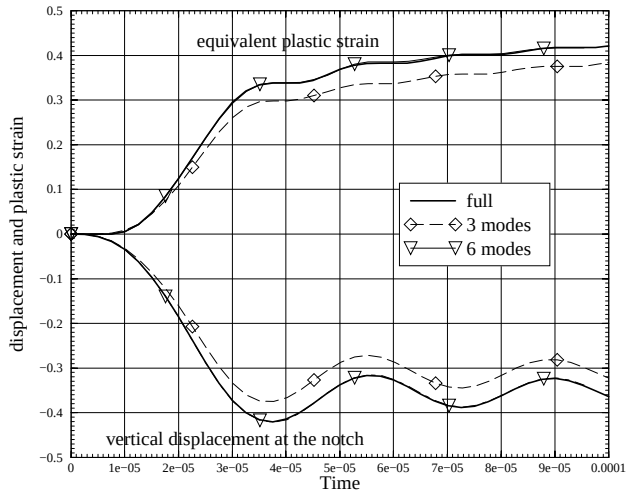

Figure 15. Elastoplastic deformation of notched beam. Deflection and equivalent plastic strain in the notch.

Copyright © 2000 John Wiley & Sons, Ltd.

Prepared using nmeauth.cls

be expressed in a much smaller number of approximation basis functions than are contained in the underlying FE model. That enables considerable savings in computing time and storage. The presented approach shares features with the well-known principle of modal superposition, which is often used in linear FE dynamics and in incremental formulations of non-linear FE models. However, in contrast to the traditional approach, the optimal representation preserves the mechanical structure of the unreduced FE model, and the basis is derived from a statistical viewpoint: the overall, global response of the full model is closely approximated in a statistical sense by the reduced model. In other words, a linear subspace of the configuration space is identified such that it matches the subset of the configuration space in which the response of the full model is expected to be located. Furthermore, the time stepping is performed entirely in terms of the primary unknowns (FE displacements), and only the solution for the incremental quantities is cast in the reduced space. The above properties, and the fact that the optimal representation does not need to be updated during the simulation, lead to increased robustness and flexibility, and allows for more effective control of the truncation error.

The reduced basis is derived by resorting to a well-known statistical theory of empirical eigenvector (EE) basis (also known as principal components or factor analysis, proper orthogonal decomposition, Karhunen-Loève expansion, and total least squares). It is shown that the EE basis has certain optimality properties, which enable the algorithm to dispense with the usual cost of solving an eigenvibration problem or of generating the Ritz or Lanczos sequence a number of times during the simulation with the reduced model. The robustness of the optimal basis is governed by the robustness of the statistical ensemble from which it was derived.

The good properties of the present approach are documented on a number of examples, and even though the selected models are fairly small by today's standards, valuable savings in computing resources are demonstrated. Even more importantly, an optimal scalability of the overall algorithm is achieved, and execution on both shared- and distributed-memory parallel computer architectures may be expected to be scalable and very efficient.

Future Directions. Applications for the proposed methodology are numerous, for instance in design optimization, convergence analyses, design of mechanical controllers and elsewhere. Error analysis (control of the truncation error) and techniques for assessing the accuracy and robustness of the model reduced solution, as well as methods for using the computed solution to generate a more accurate solution using a higher dimensional reduced model, are currently being actively investigated.

Treatment of more general configuration manifolds, especially in conjunction with constraints (for instance, incompressibility) had been sketched in Reference [23], and is also the subject of current investigations.

An important area of adaptive methodologies may be addressed by using the empirical eigenvector (EE) basis to drive *mesh adaptation*. The EE basis identifies patterns, or modes, and the mesh may be conceivably adapted to the solution by adapting it to the major response modes.

ACKNOWLEDGEMENTS

We thank Peter Schröder, John Doyle, and Ronald Coifman for helpful comments and inspiration. The research of SL was partially supported by AFOSR MURI grant F49620-96-1-0471, that of PK was partially supported by NSF/DARPA/Opaal grant DMS-9874082 and the research of JEM was partially supported by NSF-KDI grant ATM-98-73133.

REFERENCES

1. B. O. Almroth, P. Stern, and F. A. Brogan. Automatic choice of global shape functions in structural analysis. *AIAA Journal*, 16(5):525–528, 1978.
2. E. Balmès. Parametric families of reduced finite element models. Theory and applications. *Mechanical Systems and Signal Processing*, 10(4):381–394, 1996.

Copyright © 2000 John Wiley & Sons, Ltd.

Prepared using nmeauth.cls

3. C. Cabos. Error bounds for dynamic reponses in forced vibration problems. *SIAM J. Sci. Comput.*, 15(1):1–15, 1994.
4. A. S. L. Chan and K. M. Hsiao. Nonlinear analysis using a reduced number of variables. *Computer Methods in Applied Mechanics and Engineering*, 52:899–913, 1985.
5. C. Chang and J. J. Engblom. Nonlinear dynamical response of impulsively loaded structures: A reduced basis approach. *AIAA J.*, 29(4):613–618, 1991.
6. A. Dür. On the optimality of the discrete Karhunen-Loève expansion. *SIAM J. Control. Optim.*, 36(6):1937–1939, 1998.
7. D. F. Enns. *Model reduction for control system design.* PhD thesis, Stanford university, 1984.
8. K. Fukunaga. *Introduction to statistical pattern recognition.* Academic Press, Inc., 1972.
9. K. Glover. All optimal Hankel-norm approximations of linear multivariable systems and their L-infinity error bounds. *International Journal of Control*, 39:1115–1193, 1984.
10. G. H. Golub and C. F. van Loan. *Matrix computations.* Oxford: North Oxford Academic, 1983.
11. H. Harman. *Modern factor analysis.* University of Chicago Press, 1960.
12. P. Holmes, J. L. Lumley, and G. Berkooz. *Turbulence, coherent structures, dynamical systems and symmetry.* Cambridge University Press, 1996.
13. H. Hotelling. Analysis of complex statistical variables in principal components. *J. Exp. Psy.*, 24:417, 1953.
14. A. Ibrahimbegovic and E. L. Wilson. Automated truncation of Ritz vector basis in modal transformation. *J. Engineering Mechanics ASCE*, 116(11):2506–2520, 1990.
15. S. R. Idelsohn and A. Cardona. A load-dependent basis for reduced nonlinear structural dynamics. *Computers and Structures*, 20(1–3):203–210, 1985.
16. S. R. Idelsohn and A. Cardona. A reduction method for nonlinear structural dynamics analysis. *Computer Methods in Applied Mechanics and Engineering*, 49:253–279, 1985.
17. K-J. Joo and E. L. Wilson. An adaptive finite element technique for structural dynamic analysis. *Computers and Structures*, 30(6):1319–1339, 1988.
18. K-J. Joo, E. L. Wilson, and P. Leger. Ritz vectors and generation criteria for mode superposition analysis. *Earthquake Engineering and Structural Dynamics*, 18:149–167, 1989.
19. C. Kane, J. E. Marsden, M. Ortiz, and M. West. Variational integrators and the Newmark algorithm for conservative and dissipative mechanical systems. To appear, *Intern. J. for Num. Meth. in Engin.*, 1999.
20. K. Karhunen. Zur Spektraltheorie stochastischer Prozesse. *Ann. Acad. Sci. Fennicae*, 37, 1946.
21. K. A. Kline. Dynamic analysis using a reduced basis of exact modes and Ritz vectors. *AIAA Journal*, 24(12):2022–2029, 1986.
22. E. Kreuzer and O. Kust. Analysis of long torsional strings by proper orthogonal decomposition. *Archive of Applied Mechanics*, 67:68–80, 1996.
23. S. Lall, P. Krysl, and J. E. Marsden. Structure-preserving model reduction of mechanical systems. In Preparation, 2000.
24. P. Leger and S. Dussault. Non-linear seismic response analysis using vector superposition methods. *Earthquake Engineering and Structural Dynamics*, 21:163–176, 1992.
25. M. M. Loève. *Probability theory.* Van Nostrand, N. J., 1955.
26. E. N. Lorenz. Empirical orthogonal eigenfunctions and statistical weather prediction. Technical report, MIT, Department of Meteorology, 1956. Statistical forecasting project.
27. J. L. Lumley. The structure of inhomogeneous turbulent flows. In A. M. Yaglom and V. I. Tatarski, editors, *Atmospheric turbulence and radio wave propagation*, pages 166–178. Nauka, Moscow, 1967.
28. J. E. Marsden and T. J. R. Hughes. *Mathematical Foundations of Elasticity.* Dover Publications, New York, 1983.
29. Multiresolution Simulation & Engineering Design Project Web Site, *http://www.mrsed.caltech.edu.*
30. R. E. Nickell. Nonlinear dynamics by mode superposition. *Computer Methods in Applied Mechanics and Engineering*, 7:107–129, 1976.
31. A. K. Noor. Recent advances in reduction methods for nonlinear problems. *Computers and Structures*, 13:31–44, 1981.
32. A. K. Noor and J. M. Peters. Reduced basis technique for nonlinear analysis of structures. *AIAA Journal*, 18(4):455–462, 1980.
33. K. Pearson. On lines and planes of closest fit to systems of points in space. *Philo. Mag.*, 6:559, 1901.
34. J. M. Ricles and P. Leger. Use of load-dependent vectors for dynamic analysis of large space structures. *Comm. Num. Meth. Engineering*, 9:897–908, 1993.
35. J. M. A. Scherpen. H-infinity balancing for nonlinear systems. *International Journal of Robust and Nonlinear Control*, 6:645–668, 1996.
36. E. Schmidt. Zur Theorie der linearen und nichtlinearen Integralgleichungen. I Teil: Etwicklung willkürlicher Funktion nach Systemen Vorgeschriebener. *Mathematische Annalen*, 63:433–476, 1907.
37. J. C. Simo and T. J. R. Hughes. *Computational Inelasticity.* Springer Verlag, New York, 1998.

Copyright © 2000 John Wiley & Sons, Ltd.

Prepared using nmeauth.cls

38. L. Sirovich. Turbulence and the dynamics of coherent structures. I. Coherent structures. *Q. Appl. Math.*, 45:561–571, 1987.
39. L. Sirovich. Turbulence and the dynamics of coherent structures. II. Symmetries and transformations. *Q. Appl. Math.*, 45:573–582, 1987.
40. L. Sirovich. Turbulence and the dynamics of coherent structures. III. Dynamics and scaling. *Q. Appl. Math.*, 45:583–590, 1987.
41. L. Sirovich and R. Everson. Management and analysis of large scientific datasets. *Int. J. Supercomputer Applications*, 6(1):50–68, 1992.
42. J. A. Stricklin, J. E. Martinez, J. K. Tillerson, J. H. Hong, and W. E. Haisler. Nonlinear dynamic analysis of shells of revolution by matrix displacement method. *AIAA Journal*, 9(4):629–636, 1971.
43. D. Tao and E. Ramm. Characteristics of subspace in reduced basis technique. *International Journal for Numerical Methods in Engineering*, 31:1567–1583, 1991.
44. E. L. Wilson, M. W. Yuan, and J. M. Dickens. Dynamic analysis by direct superposition of Ritz vectors. *Earthquake Engineering and Structural Dynamics*, 10:813–821, 1982.
45. G. Wood, P. J. Goddard, and K. Glover. Approximation of linear parameter-varying systems. In *Proceedings of the IEEE Conference on Decision and Control*, 1996.
46. H. Xia and J. L. Humar. Frequency dependent Ritz vectors. *Earthquake Engineering and Structural Dynamics*, 21:215–231, 1992.

Copyright © 2000 John Wiley & Sons, Ltd.

Prepared using nmeauth.cls

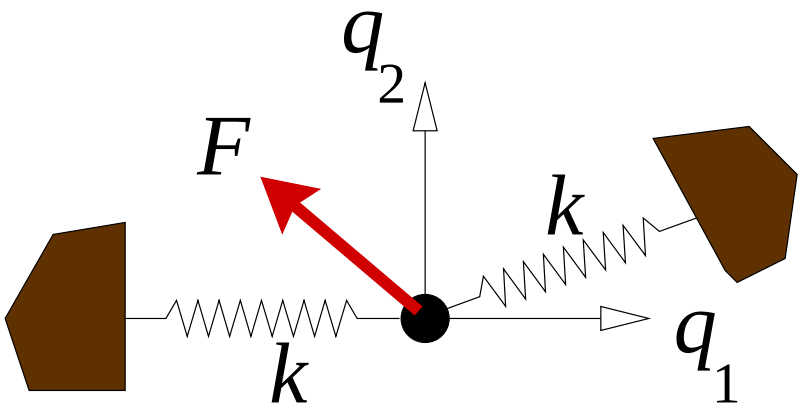

Copyright © 2000 John Wiley & Sons, Ltd.
Prepared using nmeauth.cls

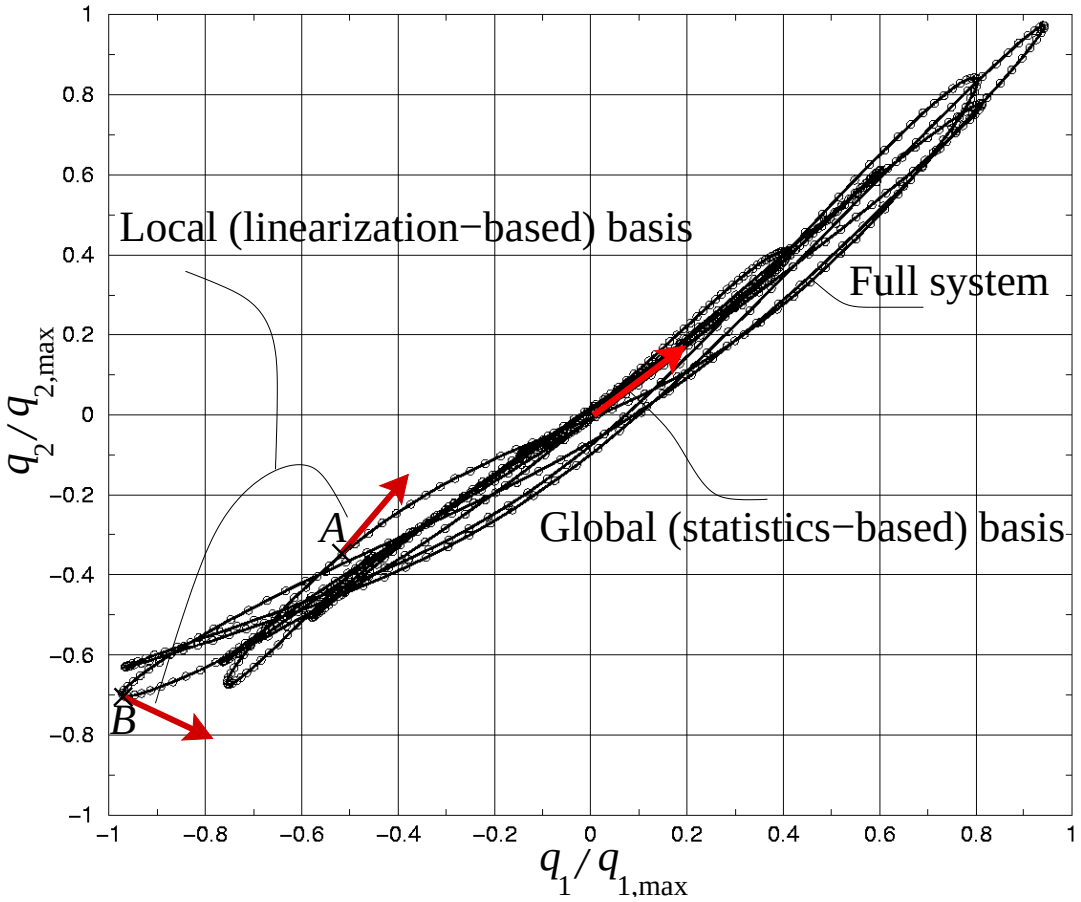

Copyright © 2000 John Wiley & Sons, Ltd.
Prepared using nmeauth.cls

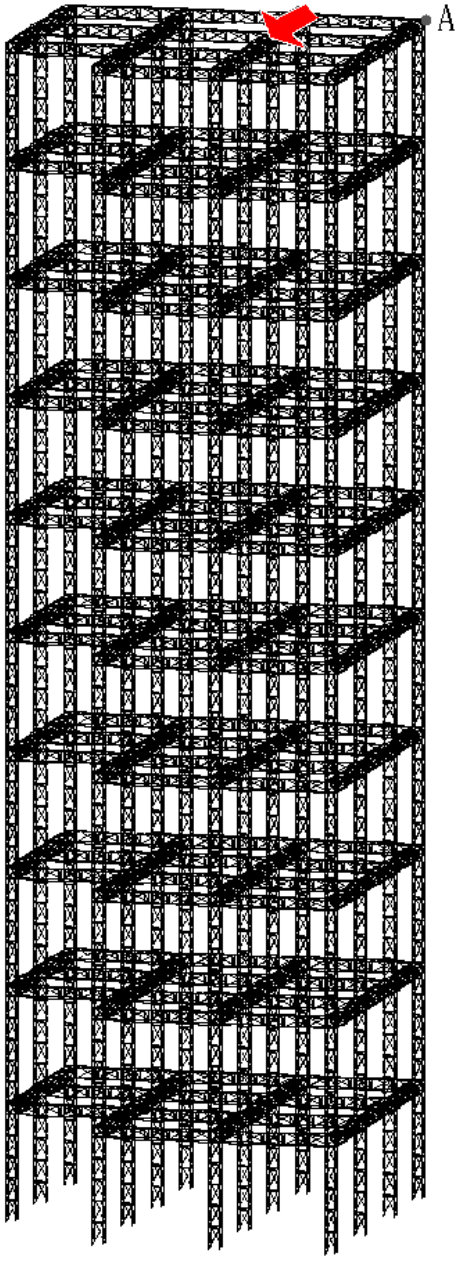

Copyright © 2000 John Wiley & Sons, Ltd.
Prepared using nmeauth.cls

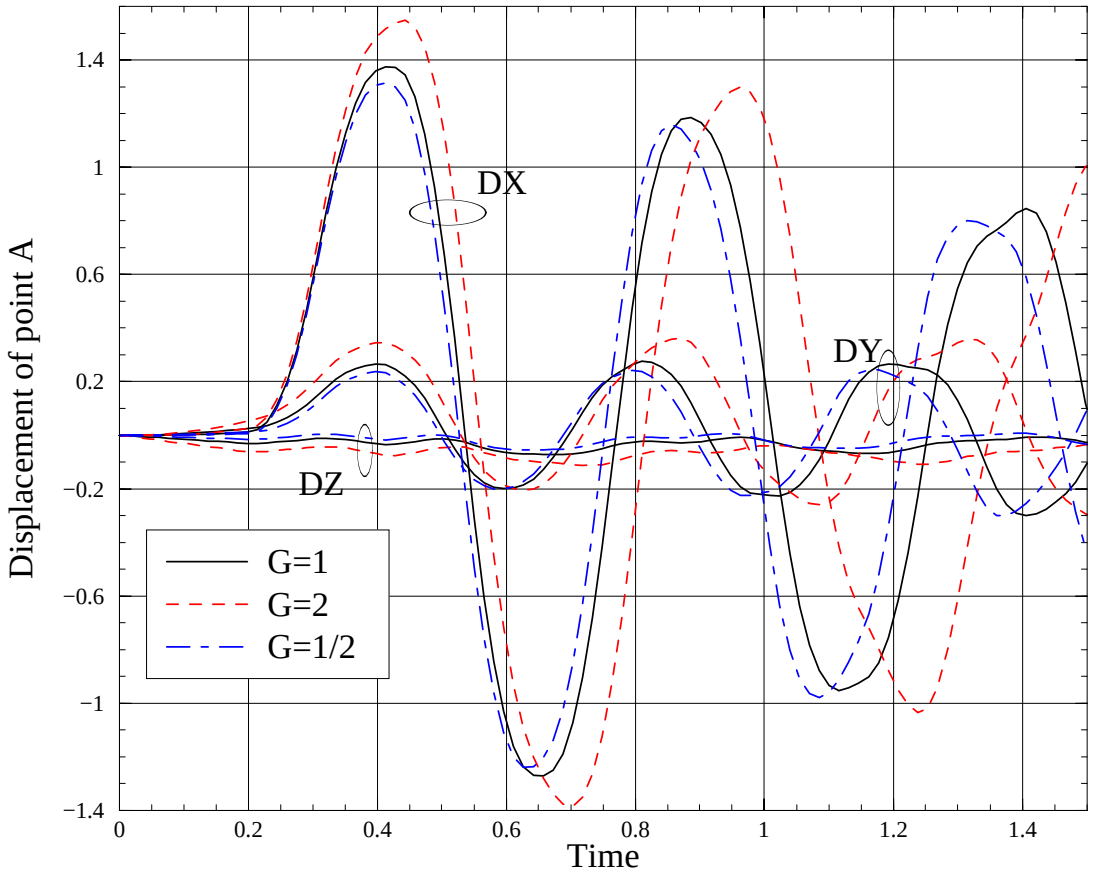

Copyright © 2000 John Wiley & Sons, Ltd.
Prepared using nmeauth.cls

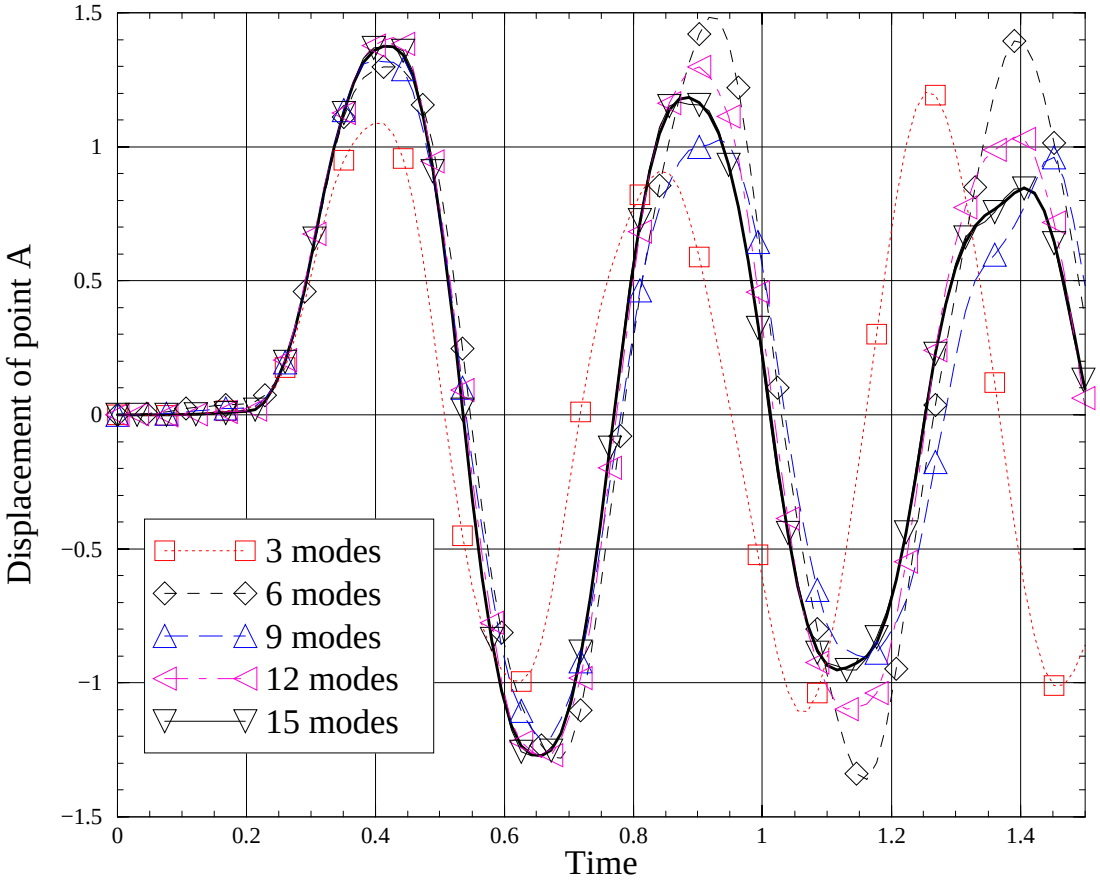

Copyright © 2000 John Wiley & Sons, Ltd.

Prepared using nmeauth.cls

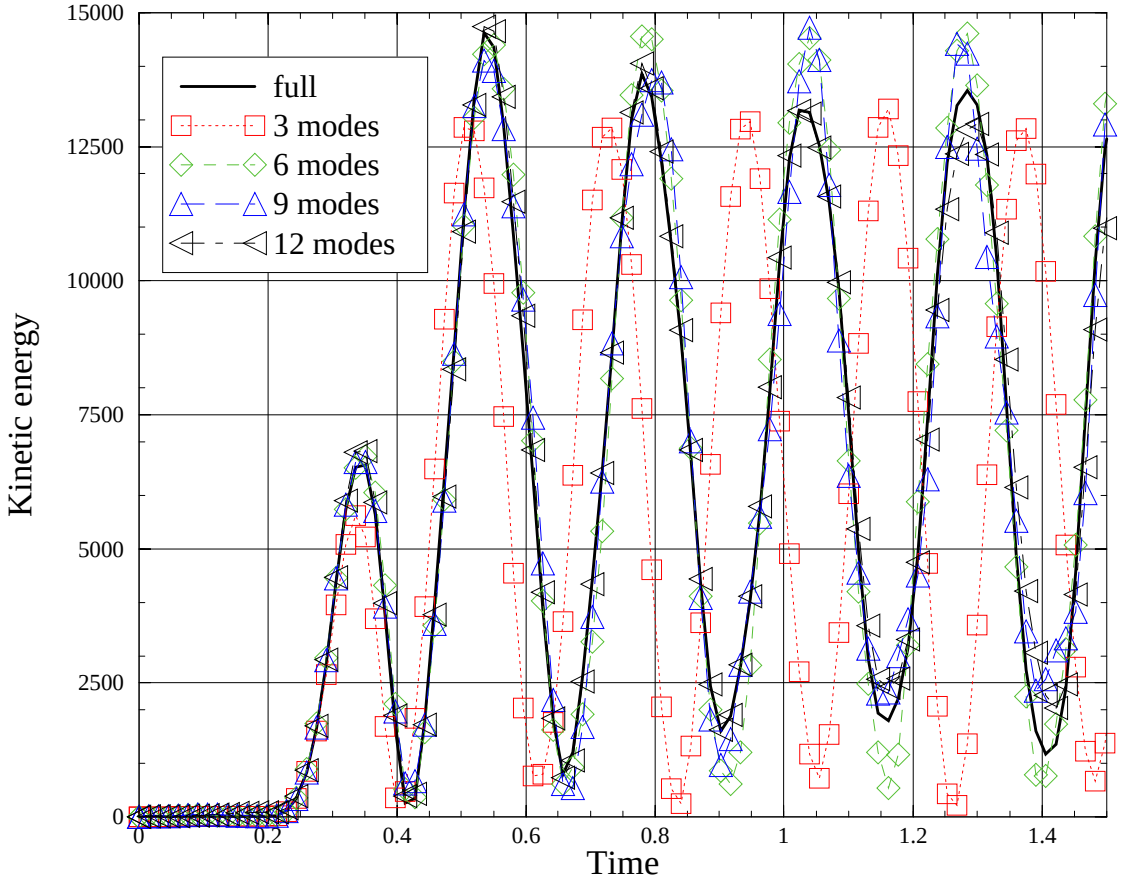

Copyright © 2000 John Wiley & Sons, Ltd.

Prepared using nmeauth.cls

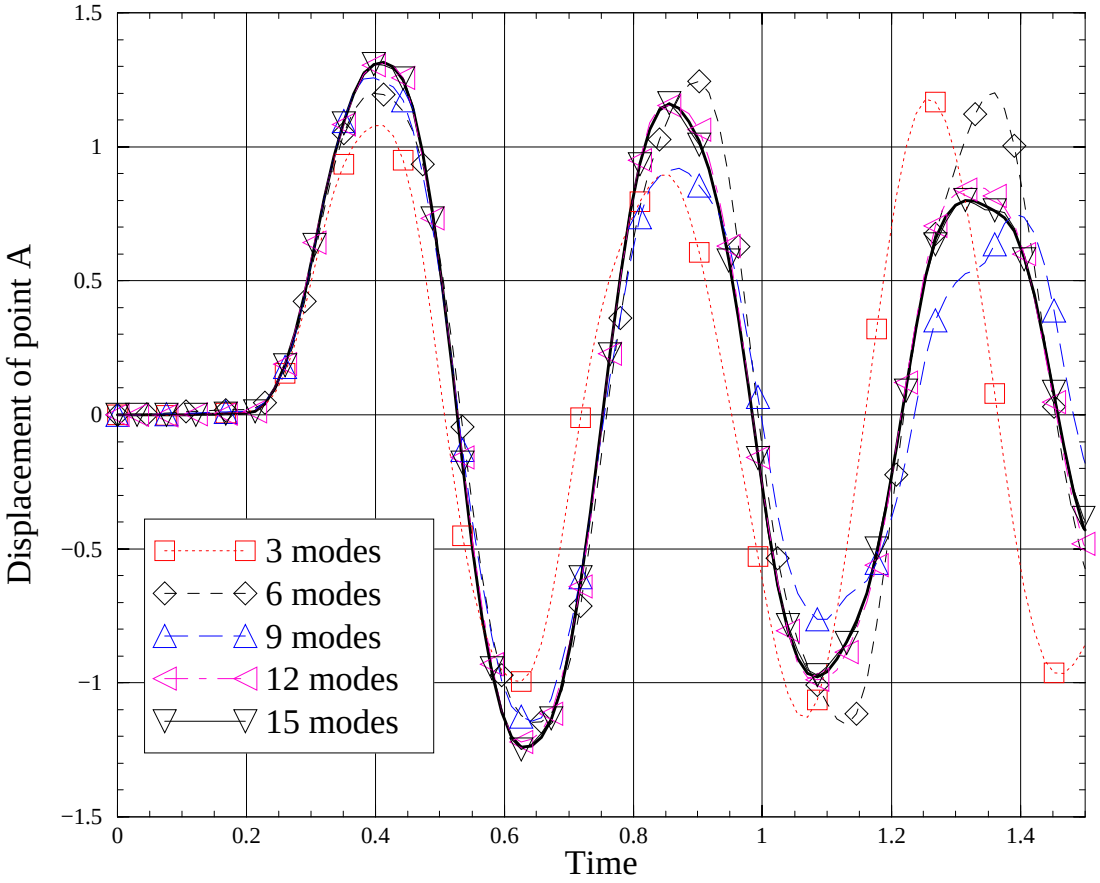

Copyright © 2000 John Wiley & Sons, Ltd.

Prepared using nmeauth.cls

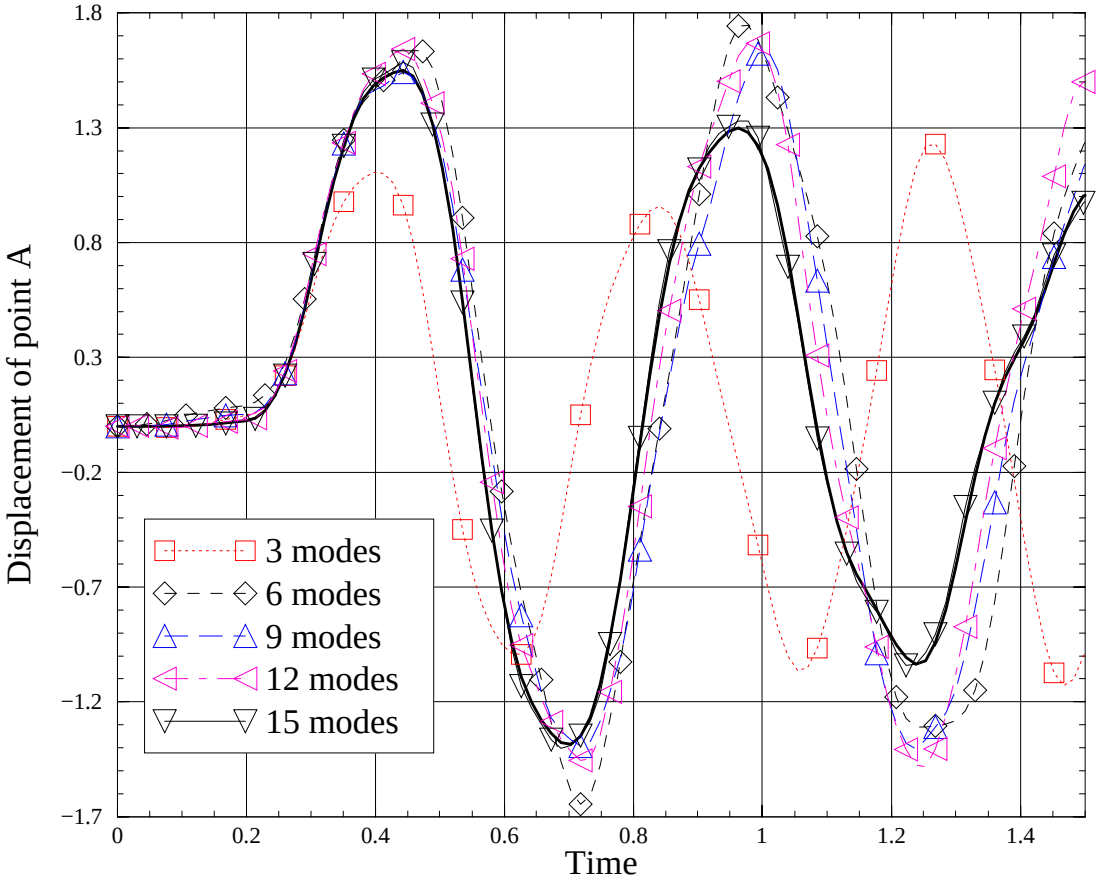

Copyright © 2000 John Wiley & Sons, Ltd.
Prepared using nmeauth.cls

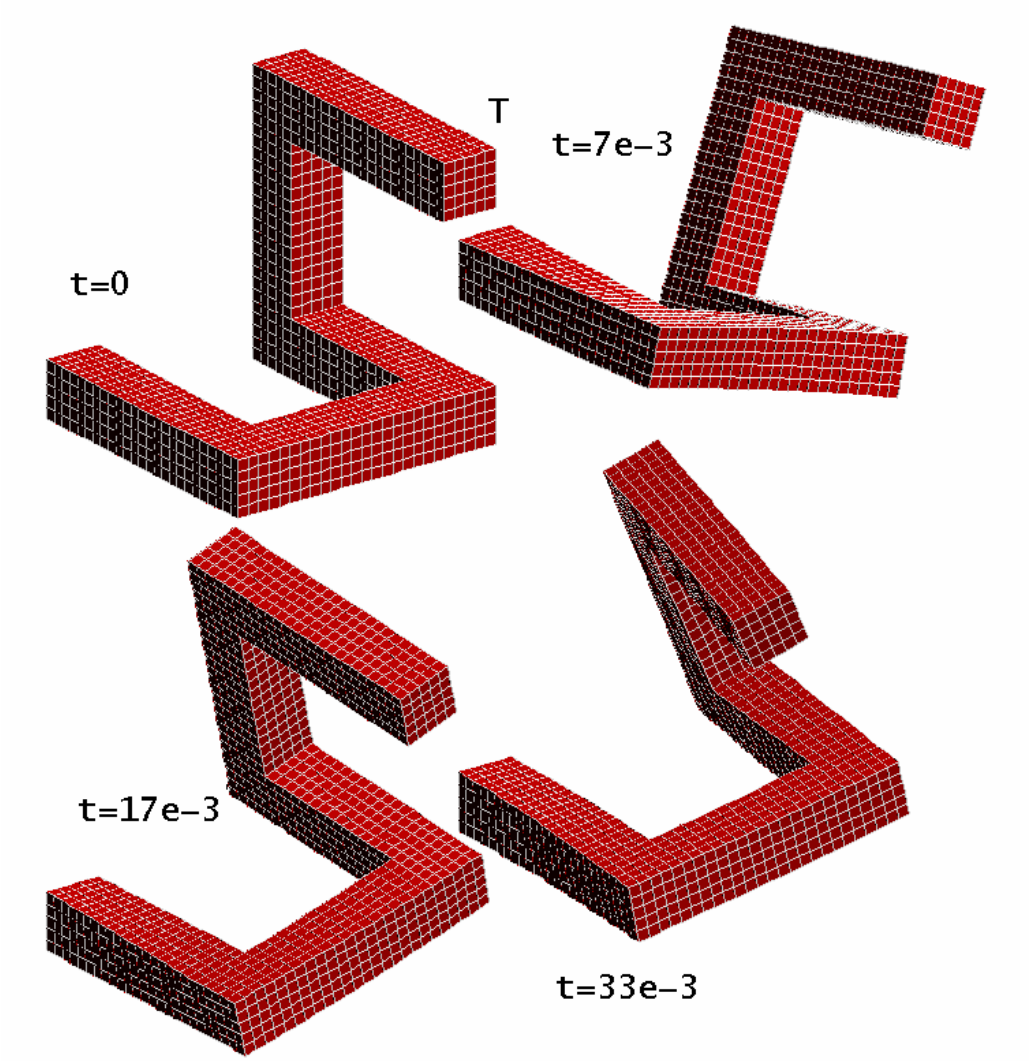

Copyright © 2000 John Wiley & Sons, Ltd.

Prepared using nmeauth.cls

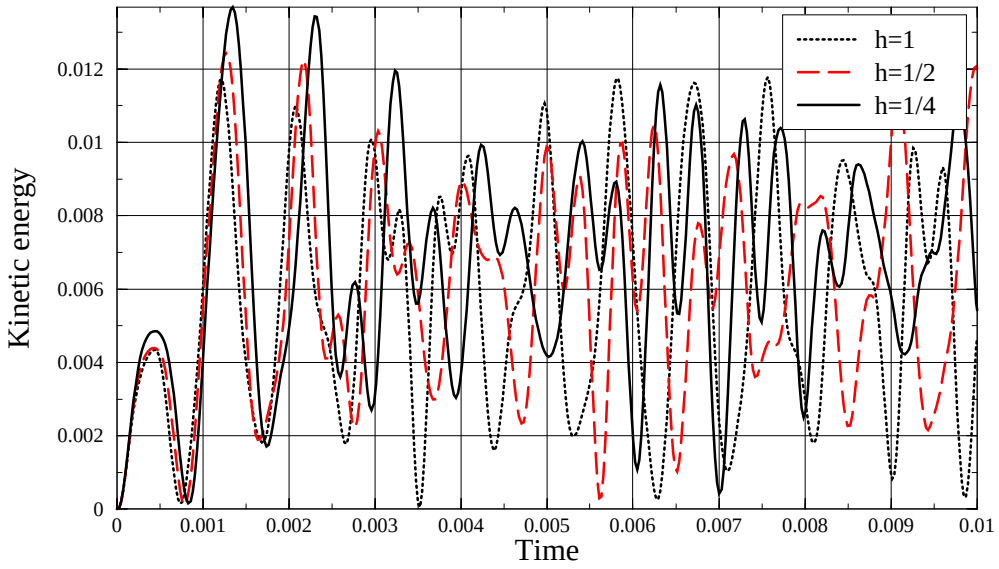

Copyright © 2000 John Wiley & Sons, Ltd.

Prepared using nmeauth.cls

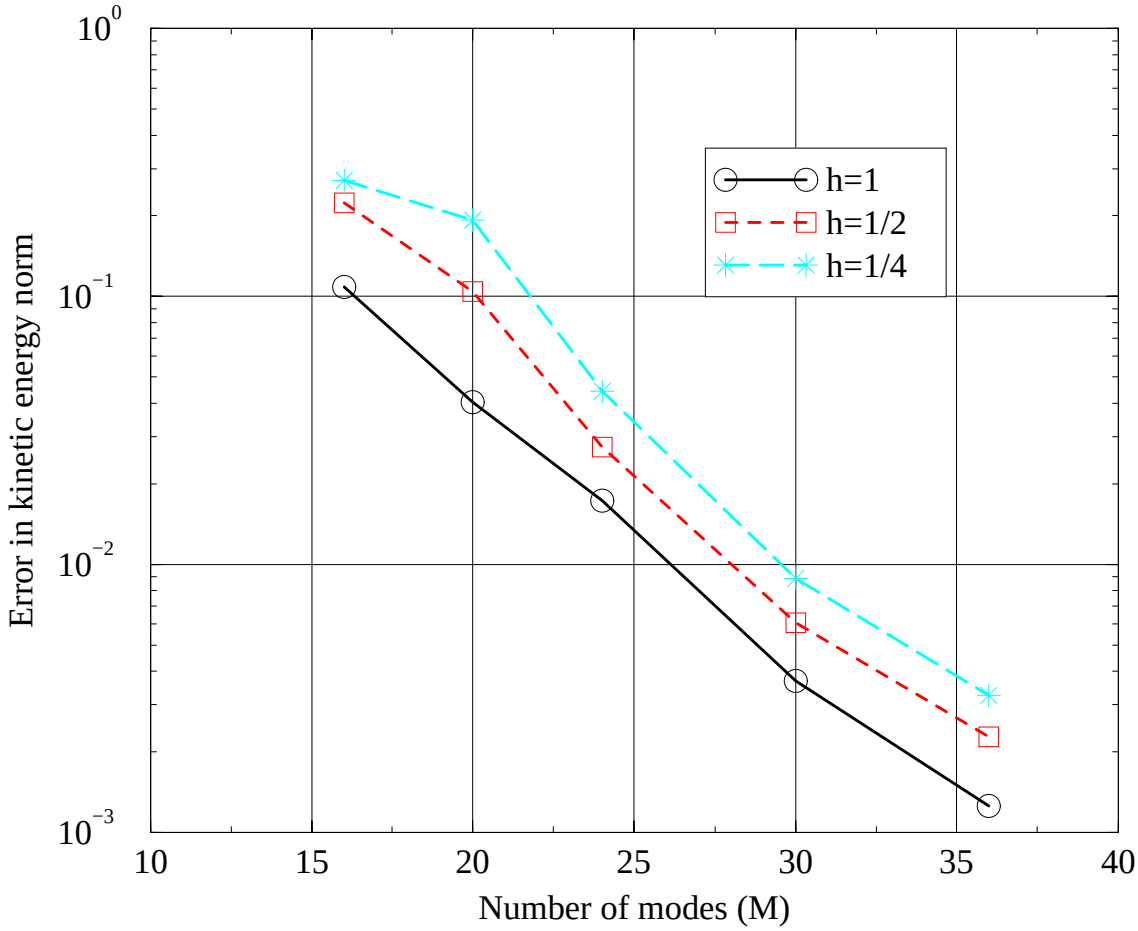

Copyright © 2000 John Wiley & Sons, Ltd.

Prepared using nmeauth.cls

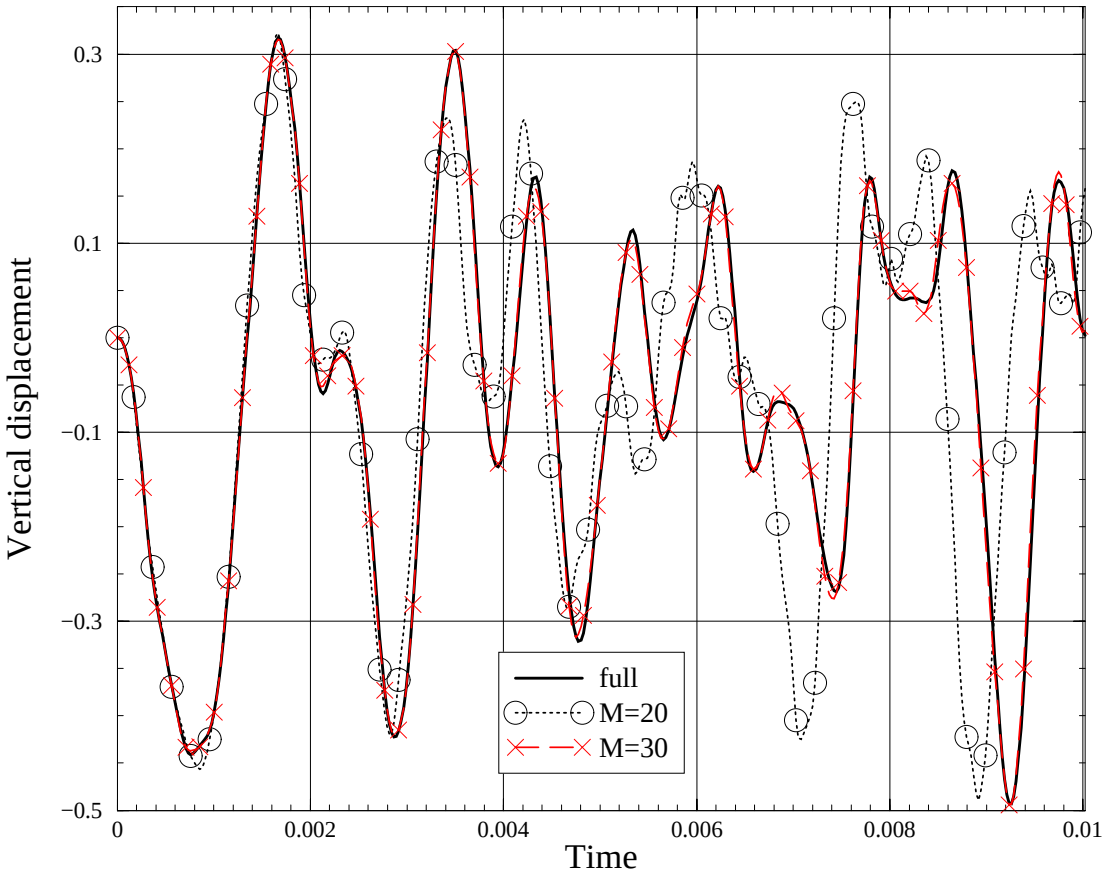

Copyright © 2000 John Wiley & Sons, Ltd.

Prepared using nmeauth.cls

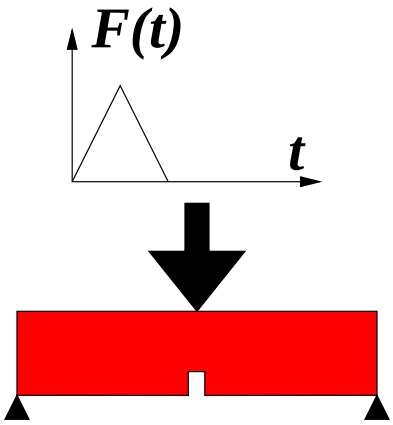

Copyright © 2000 John Wiley & Sons, Ltd.
Prepared using nmeauth.cls

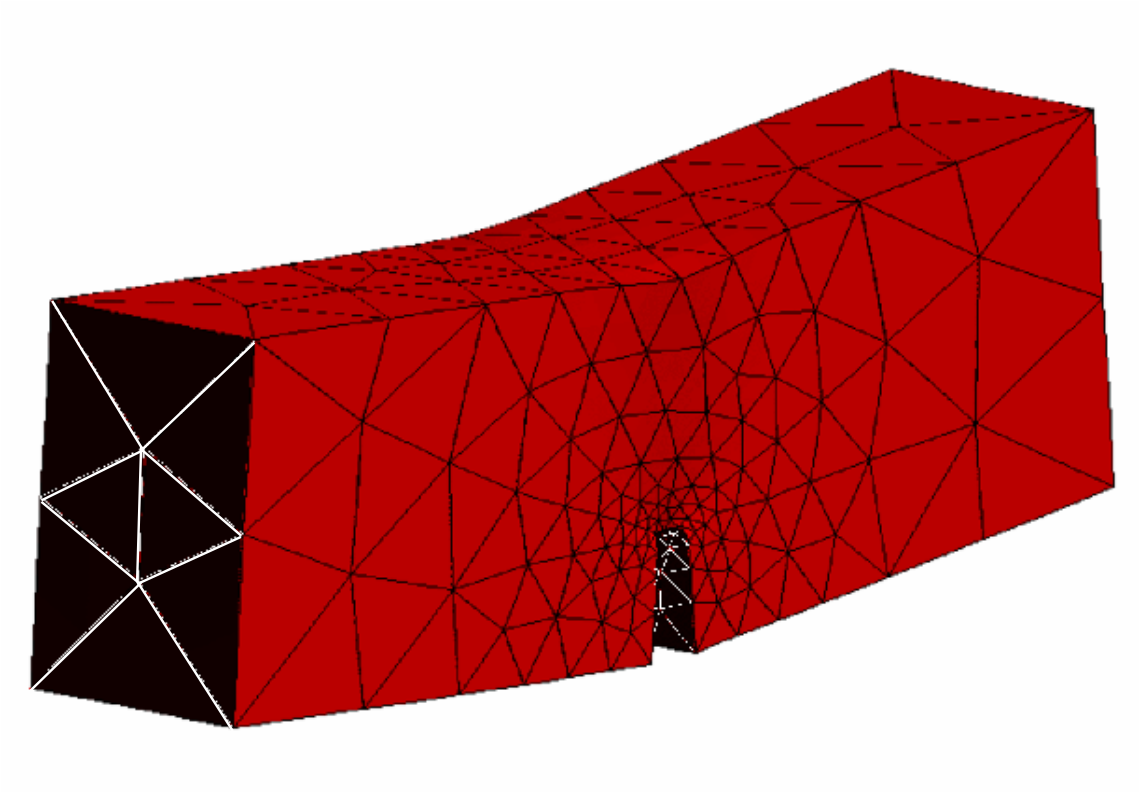

Copyright © 2000 John Wiley & Sons, Ltd.
Prepared using nmeauth.cls

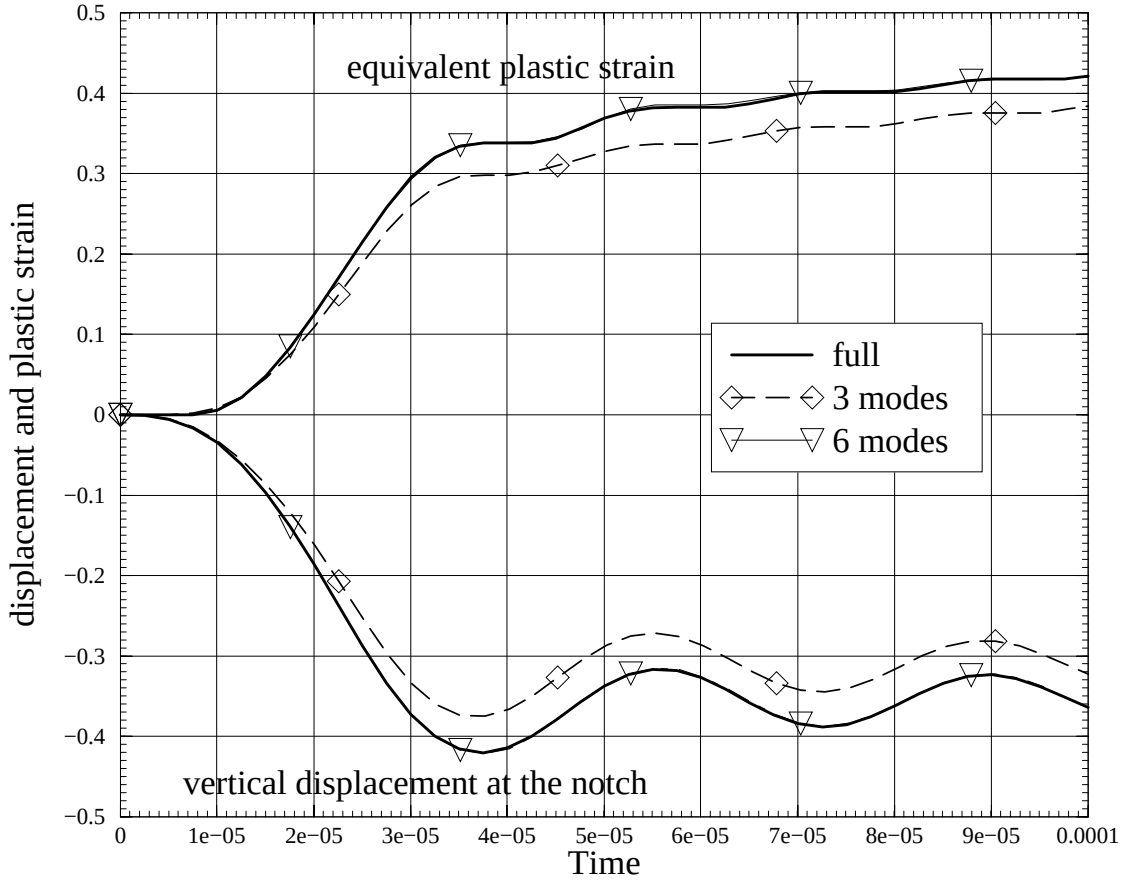

Copyright © 2000 John Wiley & Sons, Ltd.

Prepared using nmeauth.cls

Figure captions

Figure 1. Concentrated mass supported by two springs with elastic constant k in a plane. Forcing: $F_i(t) = \widehat{F}_i \cos(\omega_i t + \psi_i)$, $\omega_1 \neq \omega_2$, $\psi_1 \neq \psi_2$. Displacements are on the order of one fifth of the length of the springs.

Figure 2. Comparison of local (linearization-based) reduced basis and global (statistics-based) reduced basis for a two-degree-of-freedom mechanical system.

Figure 3. Tall truss frame structure.

Figure 4. Response of the full system for different magnitudes of the vertical load.

Figure 5. Tall truss frame. Displacement of point A in the direction of the horizontal load for $g = 1$.

Figure 6. Tall truss frame. Kinetic energy for $g = 1$.

Figure 7. Tall truss frame. Displacement of point A in the direction of the horizontal load for $g = 1/2$.

Figure 8. Tall truss frame. Displacement of point A in the direction of the horizontal load for $g = 2$.

Figure 9. Selected shapes of the spatial frame during the simulation (FE model $h = 1/4$).

Figure 10. Spatial frame. Kinetic energy computed with full FE models.

Figure 11. Spatial frame. Convergence in the kinetic energy.

Figure 12. Vertical displacement of point T for $h = 1/4$. Full and reduced models.

Figure 13. Elastoplastic deformation of notched beam. Problem setup.

Figure 14. Elastoplastic deformation of notched beam. Deformed mesh at the end of the simulation. Actual scale.

Figure 15. Elastoplastic deformation of notched beam. Deflection and equivalent plastic strain in the notch.

Copyright © 2000 John Wiley & Sons, Ltd.

Prepared using nmeauth.cls